

See discussions, stats, and author profiles for this publication at: <https://www.researchgate.net/publication/252841612>

A GRADIENT BASED OPTIMISATION ALGORITHM FOR THE DESIGN OF BRASS-WIND INSTRUMENTS

Article

CITATIONS

15

READS

1,083

1 author:



J. O. Daniel Noreland

Skogforsk

28 PUBLICATIONS 607 CITATIONS

SEE PROFILE

A GRADIENT BASED OPTIMISATION ALGORITHM FOR THE DESIGN OF BRASS-WIND INSTRUMENTS

DANIEL NORELAND*

Abstract. This paper presents how the shape of a brass instrument can be optimised with respect to its intonation and impedance peak magnitudes. The instrument is modelled using a one-dimensional transmission line analogy with truncated cones. The optimisation employs the Levenberg-Marquardt method, with the gradient of the objective function obtained by analytic manipulation. Through the use of an appropriate choice of design variables, the optimisation is capable of rapidly finding smooth horn profiles.

Key words. Shape optimisation, brass instrument, acoustic horn, Webster's horn equation.

1. Introduction. The process that governs sound generation in brass instruments has attracted much attention over the past decades. With the mathematical tools that have been developed for the analysis of brass instruments it is possible to acquire rather precise knowledge about the properties of an instrument, even before it is constructed. A problem that has started to attract interest recently, is the task to design an instrument with a prescribed set of acoustic properties. Another slightly less demanding, but more common and equally important task, is to identify and remedy imperfections of an already existing instrument. Although the quality of a musical instrument is in several aspects subjective and difficult to quantify, factors such as intonation, responsiveness and tonal colour can be attributed to well established physical properties of the instrument. Of these properties, the input impedance spectrum is the single most important entity for a brass instrument. The modulus of the input impedance exhibits a number of more or less sharp peaks, and in order to achieve good intonation and stability of a played note, the frequencies of the peaks should match those of the note and its harmonics. The absolute peak levels and bandwidths are also important in that they affect the stability of the notes [4], [13], as well as the tonal colour. A high and sharp peak “locks” the frequency of a note more efficiently than does a low and dull peak, which renders the note unstable and wobbly. Instability may also stem from misalignment between the harmonics of the tone and the corresponding impedance peaks. A pronounced example of this phenomenon is observed in the brass instruments within the cylindrical family, such as the trumpet. The first impedance peak of these instruments does not fit into the nearly harmonical sequence formed by the other peaks. Consequently, the corresponding pedal-note is considerably wobbly and difficult to play.

A real brass instrument is a complex construction both geometrically and

¹Department of Information Technology, Uppsala University, Box 337, SE-751 05 Uppsala, Sweden.

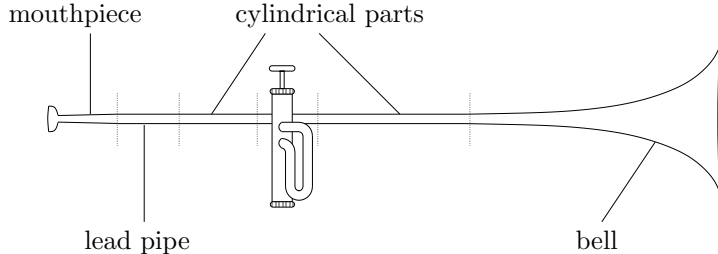


FIG. 1. *An imagined brass instrument subject to localised optimisation.*

acoustically. On a trumpet, seven different valve combinations are used — each of which actually can be said to constitute an instrument of its own. Altering e.g. the bell will thus have to be done in a way that gives the desired performance for all the seven different instruments simultaneously.

Unless the goal is to create some new and exotic instrument, the design process is usually not intended to regard the dimensions of every acoustically influential part as a free parameter. Rather, the optimisation will affect only a few selected parts of the geometry. When an instrument is constructed, it is of course advantageous to use standard components as far as possible. There are valves, water keys and other components that have a more or less predefined shape. Furthermore, all brass instruments contain at least some cylindrical sections, if not for any reason as parts of the tuning slides. In the instruments where the cylindrical part of the total length is considerable, small deviations from the cylindrical shape would increase the cost of manufacture substantially. Likewise, improving the intonation of an existing instrument should—needless to say—be done by identifying and altering as small a section of the instrument as possible. The bell, the lead pipe and the mouthpiece are examples of possible candidates for alterations in that case. Consider the imagined instrument of Fig. 1. The free parameters in the design of this instrument might be the geometry of the mouthpiece, the length and taper of the lead pipe, the lengths and diameter of the cylindrical parts and tuning slide and finally the shape of the bell.

There is a conceptual difference between inverse problems and shape optimisation. The solution of an inverse problem, on the one hand, regards the determination of an unknown setting from observations of its response to some stimulus. Inverse problems often rise difficult questions about existence and uniqueness of solutions. Shape optimisation, on the other hand, treats the problem of changing the shape of an object in order to optimise some of its physical properties. The question about uniqueness is usually of less concern in this case. Shape optimisation should be distinguished from topology optimisation, where also the topology of the object is free to vary.

Of interest is the work done by Amir et al. [2]. Considering wave propagation as approximately one-dimensional, they apply variations of the so-called *layer*

peeling algorithm [10], [9], in order to reconstruct the bore of acoustic horns from pulse reflectometry data. The work done by Bonder [7] regarding the identification of the shape of the glottis from the formant frequencies should also be mentioned. Although these bore reconstruction methods are useful as a non-intrusive way of measuring the internal dimensions of existing instruments – perhaps too old and fragile for handling – they are of limited value as an aid to design or intonate instruments.

Much less is reported about wind instrument optimisation in the literature. To the author’s knowledge, the only published work in this respect is a paper by [17], where genetic algorithms and the Rosenbrock minimisation procedure are used to optimise the intonation of brass instruments.

The scope of this paper is to present a fast and accurate method by which it is possible to optimise the geometry of a musical horn with respect to the frequencies and magnitudes of the peaks in the input impedance spectrum. The horns are considered to be straight, and of circular cross section. Bends and valves are not included in the model, but if pre-computed impedance matrices for such objects are available, they can easily be accounted for acoustically, if not subject to the optimisation.

2. The optimisation problem. The first step in the formulation of a shape optimisation algorithm is to define a numerical measure of the quality of a design, the *objective function*. One such measure would be the square of the L_2 -norm of the difference between the target input impedance and that of the design. If we symbolically denote the horn design by α , the objective function would be

$$J(\alpha) = \int_{-\infty}^{\infty} |Z_{in}(f; \alpha) - Z_{target}(f)|^2 df.$$

α may, for instance, denote the function that gives the radius of the horn as a function of the position along the axis of symmetry or, in the discrete case, a set of design parameters defining the horn geometry through some mathematical relation. The inverse problem of finding α_* such that $\alpha^* = \arg \min J(\alpha)$, with $J = 0$ for a noise free Z_{target} , is the most general design problem. However, in light of the foregoing discussion, a bore reconstruction of this type is often too general for instrument design or intonation purposes. From a musical point of view, the impedance peaks are usually what attracts the most interest. The impedance between the peaks is much more free to vary, since its very value is not of such great concern. This feature leaves more freedom in changing the geometry than if the whole spectrum is specified.

2.1. Objective function and optimisation strategy. The most straightforward measure of the intonation is the square sum of the deviations between the impedance peaks and their desired locations. However, in order to avoid having to explicitly find the maxima, and differentiate their locations with respect to the design variables, it is possible to use the observation that Z_{in} is real

at the maxima and minima of $|Z_{in}|$ [11]¹. Thus, the square-sum of $\text{Im}(Z_{in})$ at the desired impedance peak frequencies can be used as a measure of the deviation in intonation. It is necessary to also include the impedance levels at the peak frequencies, since otherwise the optimisation has no way of discerning the impedance maxima from the minima. The specification of the absolute level has also been shown to be necessary from another aspect. If no level is specified, the geometry will be free too attain arbitrarily wide or narrow shapes. Accordingly, if a design with n impedance peaks located at f_k , and of value Z_{peak_k} is desired, the objective function is defined as

$$J(\alpha) = \frac{1}{2} \sum_{k=1}^n \text{Im}(Z_{in}(f_k))^2 + \text{Re}(Z_{in}(f_k) - Z_{\text{peak}_k})^2 \quad (1)$$

for the design variable $\alpha \in \mathbb{R}^m$. Additional requirements, such as the value of the impedance between the peaks, can also be incorporated in J in order to adjust peak bandwidths etc.

The evaluation of the loss function for a horn is a costly operation. It is therefore necessary to employ an optimisation method that converges as quickly as possible. If the goal is to design an instrument from scratch, speed of convergence often has to be traded for robustness by using, for instance, a genetic algorithm or the Rosenbrock method [17]. However, when the design starts to converge, it is possible to use a gradient based search algorithm, which features superior convergence close to an optimum. In many practical cases, for instance when optimising the intonation, the start design is already close to an optimal design, and the gradient based method may be tried from the start. The method chosen in this work is the Levenberg-Marquardt method [20], which is a combined trust region – Gauss–Newton method that has been used successfully for many nonlinear least squares problems.

The problem at hand is conceptually a non-linear least squares problem. For such problems, the objective function J should not be computed explicitly as in (1). The least squares formulation of the design problem should instead be

$$\alpha_* = \arg \min_{\alpha \in \mathbb{R}^m} J(\alpha) = \arg \min_{\alpha \in \mathbb{R}^m} \frac{1}{2} \mathbf{F}^T \mathbf{F} \quad (2)$$

¹In the absence of a detailed model for the lip valve, the frequencies of blown notes are usually identified with the resonance frequencies observed with the mouthpiece rigidly sealed. If visco-thermal and radiation losses are present, these frequencies are in fact complex, with the imaginary part representing the damping. More specifically, the resonances are the frequencies for which the input admittance of the instrument matches the admittance of the seal, which is zero for a rigid termination. The imaginary part of these frequencies is small for weakly damped systems, and approximating the real part of the resonances with the locations of the impedance peaks (or zeros of the imaginary part) along the real ω -axis is good, although not strictly valid. This seems to be an often overlooked fact in the literature on wind instruments. The true expression for the frequency of a blown note would have to involve properties of the lip valve, as well as the input impedance of the instrument.

where

$$\mathbf{F} = \begin{bmatrix} \text{Im}(Z_{in}(f_1)) \\ \text{Re}(Z_{in}(f_1) - Z_{\text{peak}_1}) \\ \text{Im}(Z_{in}(f_2)) \\ \text{Re}(Z_{in}(f_2) - Z_{\text{peak}_2}) \\ \vdots \end{bmatrix}. \quad (3)$$

The information supplied to the least squares solver is mainly the function $\mathbf{F}(\alpha)$ and its gradient $\nabla \mathbf{F}(\alpha)$. Note that $\nabla \mathbf{F}$ requires the shape derivatives of Z_{in} .

3. The mathematical model. The second step is to formulate the mathematical model by which Z_{in} is computed. After due discretisation, the shape derivatives are found by differentiating the expression for Z_{in} w.r.t the discretisation points.

3.1. Webster's horn equation. The work in this article based on the assumption that wave propagation in a horn is approximately one-dimensional, and can be described by *Webster's horn equation*. In fact, any one-parameter acoustic field obeys this equation [25]. Assuming the usual $e^{i\omega t}$ -dependence, the horn equation reads

$$p''(z) + \frac{S'(z)}{S(z)}p'(z) + k^2p(z) = 0, \quad k = \omega/c. \quad (4)$$

Here, the coordinate z is the position along the horn axis at which it is intersected by the acoustic equi-phase surfaces, or more loosely, the wavefronts. S denotes the area of these wavefronts, ω the angular frequency, and c the speed of sound. The exact shape of the wavefronts is not known beforehand, but will be somewhere between planar and spherical [5]. For slowly flaring horns, either of these two assumptions is a good approximation, however. A thorough derivation of (4) using perturbation methods is carried out in [26].

An analytic solution to (4) in closed form can be obtained for cylinders, cones with planar or spherical wavefronts and exponential horns with planar wavefronts. For other horn contours and wavefront shapes, classical methods for the solution of Sturm-Liouville problems, such as the WKB approximation, can be used.

3.2. The input impedance and the transfer matrix of a horn. The way in which a tone is produced can only be understood by considering the interaction between the player's lips and the instrument. Put under air pressure from the oral cavity, the lips work as a pressure controlled valve, an active component that together with the instrument form an oscillator [4]. The instrument's part of the interaction is contained in the input impedance spectrum. The input impedance can be interpreted as the transfer function from the acoustic volume

flow velocity, $U_{in}(\omega)$, to the acoustic pressure, $p_{in}(\omega)$, at the mouthpiece of the instrument;

$$p_{in}(\omega) = Z_{in}(\omega)U_{in}(\omega).$$

The instrument can also be interpreted as an impedance transformer inserted between the player and the surrounding space of air. With

$$\mathbf{H} = \begin{bmatrix} H_{11} & H_{12} \\ H_{21} & H_{22} \end{bmatrix}$$

denoting the transfer matrix of the instrument, the input impedance seen from the mouthpiece is given by

$$Z_{in} = \frac{H_{12} + H_{11}Z_L}{H_{22} + H_{21}Z_L},$$

where Z_L is the radiation impedance seen from the end of the horn. The difficulties in obtaining an analytic approximation of Z_L , and numerical methods that give better approximations, are discussed in [21], but there are fairly accurate approximations, such as those in [6, p. 125] and [18].

3.3. Phase–Magnitude relation of Z_{in} . A question that is sometimes disputed is whether both phase and magnitude of the input impedance need be specified. Fortunately, these quantities are not independent of each other, but related through the *Hilbert transform*. This is a fundamental property of a causal and stable system. Assume that wave propagation in the mouthpiece of the horn is mono-modal, meaning that only the planar mode is prevalent here. Assume also that non-linear acoustic effects are negligible in the instrument. We can then state the following;

PROPOSITION 3.1. *Let $G(\omega) = |Z_{in}(\omega)|$. Then*

$$\arg(Z_{in}(\omega)) = (\text{CPV}) \frac{\omega}{\pi} \int_{-\infty}^{\infty} \frac{\ln G(\omega')}{\omega'^2 - \omega^2} d\omega'.$$

Here CPV denotes the Cauchy Principal Value, in turn defined by

$$(\text{CPV}) \int_{-\infty}^{\infty} f(x) dx = \lim_{R \rightarrow \infty} \int_{-R}^R f(x) dx.$$

This can be understood from physical arguments that are by necessity true, although not trivially seen from the wave equation and its boundary conditions. In fact, a naïvely formulated boundary condition for a wave propagation problem might violate fundamental physical properties such as conservation of energy or causality. Let us for a moment expand the definition of p , U and Z to also include

imaginary values of ω . Looking into the input of the instrument, we have a linear single input–single output system from U to p with transfer function Z_{in} ,

$$p_{in}(\omega) = Z_{in}(\omega)U_{in}(\omega).$$

Assume that we can write

$$Z_{in}(\omega) = \frac{P(\omega)}{Q(\omega)},$$

where $P(\omega)$ and $Q(\omega)$ are polynomials in ω . The rational form of $Z_{in}(\omega)$ is hypothetical for a real instrument, but we assume that the input impedance can be approximated arbitrarily well by a rational transfer function, possibly of very high order. Since the instrument is a passive and causal system, $Z_{in}(\omega)$ must correspond to a stable system, and hence, there must be no poles of Z_{in} in the lower half plane. The same argument is valid for the inverse system

$$U_{in}(\omega) = Y_{in}(\omega)p_{in}(\omega) = Z_{in}^{-1}(\omega)p_{in}(\omega),$$

and thus, $Y_{in}(\omega)$ must not have any poles in the lower half of the ω -plane. Hence we conclude that $Z_{in}(\omega)$ has neither poles nor zeros in the lower half plane. Such a system is called *minimum-phase-shift*. In a minimum-phase-shift system, the real and imaginary parts of the transfer function constitute a Hilbert transform-pair [23, p. 206]. This shows that (3.1) is valid.

Since the phase can be retrieved from the magnitude, or the imaginary part from the real part, it is in principle a matter of convenience which one of these entities to use as the observation variable in the objective function.

3.4. Numerical model of the horn equation. An established numerical method for the solution of (4) is the transmission line (TL) model, where the instrument is regarded as a series of cylindrical or conical sections [24], [11], [19]. Consider the series of conical waveguides in Fig. 2. The waveguides are numbered $1, 2, \dots, N$, and the axial positions of intersections are denoted z_1, z_2, \dots, z_{N+1} . The end diameters at these positions are denoted y_1, y_2, \dots, y_{N+1} . The transmission matrix of the whole structure can be written as the product of the individual transfer matrices \mathbf{H}_j , $j = 1, \dots, N$ of the short segments,

$$\mathbf{H}(\omega) = \prod_{j=1}^N \mathbf{H}_j(\omega; y_j, y_{j+1}, z_j, z_{j+1}). \quad (5)$$

Visco-thermal losses can conveniently be accounted for in the model. The elements of \mathbf{H}_j have been presented e.g. in [19] and [21], but are also listed in Appendix.

3.5. Convergence of the TL method. The transmission line method has been used quite extensively in the theory of musical acoustics, and also in

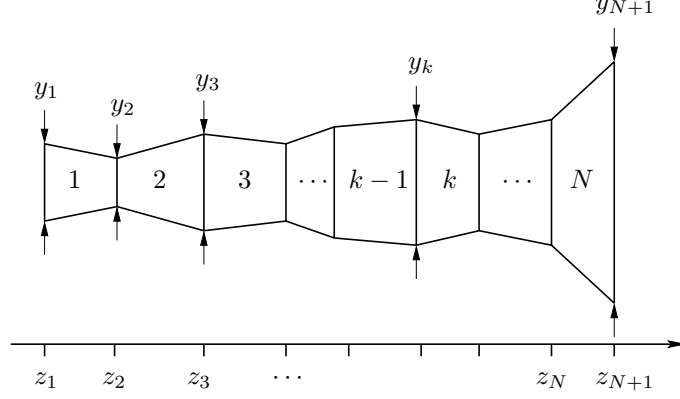


FIG. 2. The horn approximated by series of conical waveguide segments.

quantum mechanics [16]. However, the method seems to be derived rather *ad hoc*, albeit in an intuitively appealing manner. In this section a proof is presented for the convergence of the transmission line model. We restrict the argument to planar wavefront.

In this section we reserve the notations \mathbf{H}_j and \mathbf{H} for the exact entities, whereas their approximations are denoted $\tilde{\mathbf{H}}_j$ and $\tilde{\mathbf{H}}$, respectively. This distinction is otherwise not made in the text.

LEMMA 3.2. Assume that wave propagation on $z_a \leq z \leq z_b$ is described by (4), where $S(z) \in C^2$. Then there exist a unique matrix \mathbf{H} such that

$$\begin{bmatrix} p_{z_a} \\ U_{z_a} \end{bmatrix} = \mathbf{H} \begin{bmatrix} p_{z_b} \\ U_{z_b} \end{bmatrix},$$

where U_z denotes the acoustic volume flow velocity at position z .

Proof. Introduce

$$\mathbf{p}(z) = \begin{bmatrix} p(z) \\ p'(z) \end{bmatrix}.$$

We can then rewrite (4) as

$$\mathbf{p}' = \mathbf{A}(z)\mathbf{p}, \tag{6}$$

where

$$\mathbf{A}(z) = \begin{bmatrix} 0 & 1 \\ k^2 & -S'(z)/S(z) \end{bmatrix}. \tag{7}$$

The boundary conditions for (6) are written in the form

$$\mathbf{B}_{z_a}\mathbf{p}(z_a) + \mathbf{B}_{z_b}\mathbf{p}(z_b) = \mathbf{c}. \tag{8}$$

Now, let $\mathbf{p}_i(z)$, $i = 1, 2$ be the solution to the ODE $\mathbf{p}' = \mathbf{A}(z)\mathbf{p}$ with the initial value $\mathbf{p}(z_a) = \mathbf{e}_i$, where \mathbf{e}_i is the i :th column of the identity matrix. Furthermore, let $\mathbf{Y}(z)$ denote the matrix whose i :th column is given by \mathbf{p}_i . \mathbf{Y} is referred to as the fundamental solution to (4). For *fatY*, there exists an \mathbf{x} such that $\mathbf{Y}(z)\mathbf{x}$ satisfies Eq. (6) with boundary conditions (8). It is trivial to see this. \mathbf{p}_1 and \mathbf{p}_2 satisfy (6) by construction, and we see that (8) is satisfied if $\mathbf{x} = (\mathbf{B}_{z_a}\mathbf{Y}(z_a) + \mathbf{B}_{z_b}\mathbf{Y}(z_b))^{-1}\mathbf{c} = \mathbf{Q}^{-1}\mathbf{c}$. \mathbf{Q} is nonsingular if the original boundary value problem has a unique solution. With $\mathbf{p}_{z_b} = \mathbf{Y}(z_b)\mathbf{x}$, we have that $\mathbf{p}_{z_a} = \mathbf{Y}(z_a)\mathbf{x} = \mathbf{Y}(z_a)\mathbf{Y}^{-1}(z_b)\mathbf{p}_{z_b} = \tilde{\mathbf{H}}\mathbf{p}_{z_b}$. Using the identities

$$u(z) = \frac{i}{\omega\rho}p'(z), \quad U(z) = S(z)u(z), \quad (9)$$

the relation between \mathbf{p} and our original variable $[p, U]^T$ is given by

$$\begin{bmatrix} p(z) \\ U(z) \end{bmatrix} = \begin{bmatrix} 1 & 0 \\ 0 & i\frac{S(z)}{\omega\rho} \end{bmatrix} \begin{bmatrix} p(z) \\ p'(z) \end{bmatrix},$$

where ρ is the density of air. Finally, we get

$$\begin{bmatrix} p(z_a) \\ U(z_a) \end{bmatrix} = \mathbf{H} \begin{bmatrix} p(z_b) \\ U(z_b) \end{bmatrix},$$

where

$$\mathbf{H}(z_a, z_b) = \begin{bmatrix} 1 & 0 \\ 0 & i\frac{S(z_a)}{\omega\rho} \end{bmatrix} \mathbf{Y}(z_a)\mathbf{Y}^{-1}(z_b) \begin{bmatrix} 1 & 0 \\ 0 & i\frac{S(z_b)}{\omega\rho} \end{bmatrix}^{-1} \quad (10)$$

which completes the proof. \blacksquare

LEMMA 3.3. Denote by $\mathbf{H}(z_a, z_c)$ the transfer matrix for the portion of a horn between $z = z_a$ and $z = z_c$. Then

$$\mathbf{H}(z_a, z_c) = \mathbf{H}(z_a, z_b)\mathbf{H}(z_b, z_c), \quad z_a \leq z_b \leq z_c.$$

Proof. If we think of solving (6) with initial conditions from $z = z_a$ to $z = z_c$, we might as well solve from z_a to z_b and use the value of $\mathbf{y}(z_b)$ as an initial condition when solving from z_b to z_c . \blacksquare

LEMMA 3.4. Let $r(z) > 0$ define a horn contour on $z_a \leq z \leq z_a + \Delta z$ with $S(z) = \pi r^2(z)$ and Δz small. On $z_a \leq z \leq z_a + \Delta z$, $r(z)$ is approximated by

$$\tilde{r}(z) = r(z_a) + \frac{r(z_a + \Delta z) - r(z_a)}{\Delta z}(z - z_a), \quad (11)$$

and correspondingly, $\tilde{S}(z) = \pi \tilde{r}^2(z)$. The corresponding approximation $\tilde{\mathbf{H}}$ satisfies

$$\|\tilde{\mathbf{H}}(z_a, z_a + \Delta z) - \mathbf{H}(z_a, z_a + \Delta z)\| = \mathcal{O}(\Delta z^3) \quad (12)$$

Proof. We begin by recasting (4) in the form of the *Telegrapher's equation*. From the relations (9) we obtain

$$U' = \frac{iS'(z)}{\omega\rho}p' + \frac{iS(z)}{\omega\rho}p'' = -ik\frac{S(z)}{\rho c}p,$$

where the last equality was obtained by substitution of p'' from equation (4). Therefore, $[p, U]^T$ satisfies the first order system

$$\begin{bmatrix} p'(z) \\ U'(z) \end{bmatrix} = \begin{bmatrix} 0 & -ik\frac{\rho c}{S(z)} \\ -ik\frac{S(z)}{\rho c} & 0 \end{bmatrix} \begin{bmatrix} p(z) \\ U(z) \end{bmatrix},$$

which is henceforth written

$$\mathbf{p}' = -\mathbf{Z}(z)\mathbf{p}, \quad (13)$$

where $\mathbf{p} = [p, U]^T$ and

$$\mathbf{Z}(z) = \begin{bmatrix} 0 & -ik\frac{\rho c}{S(z)} \\ -ik\frac{S(z)}{\rho c} & 0 \end{bmatrix}.$$

Consider, as according to Fig. 3, the two waveguide sections between z_a and z , on the one hand, and z_a and $z + dz$ on the other hand. By Lemma 3.2 we have

$$\mathbf{p}(z_a) = \mathbf{H}(z_a, z)\mathbf{p}(z), \quad (14)$$

$$\mathbf{p}(z_a) = \mathbf{H}(z_a, z + dz)\mathbf{p}(z + dz). \quad (15)$$

From these identities, it follows that

$$\frac{d}{dz}(\mathbf{H}(z_a, z)\mathbf{p}(z)) = \frac{d}{dz}\mathbf{H}(z_a, z)\mathbf{p}(z) + \mathbf{H}(z_a, z)\mathbf{p}'(z) = 0. \quad (16)$$

Inserting (13) into (16) yields that

$$\frac{d}{dz}\mathbf{H}(z_a, z)\mathbf{p}(z) - \mathbf{H}(z_a, z)\mathbf{Z}(z)\mathbf{p}(z) = 0.$$

This equation is valid for any arbitrary $\mathbf{p}(x)$, and we may state the following ordinary differential equation for \mathbf{H} ,

$$\frac{d}{dz}\mathbf{H}(z_a, z) - \mathbf{H}(z_a, z)\mathbf{Z}(z) = 0. \quad (17)$$

Since the transmission matrix for a waveguide of zero length must equal the identity matrix, the initial value of the differential equation is

$$\mathbf{H}(z_a, z_a) = \mathbf{I}. \quad (18)$$

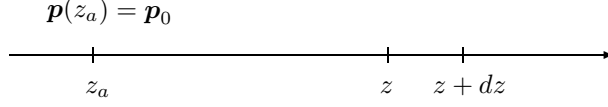


FIG. 3. Axis of symmetry along a waveguide.

Now, define the solution operator \mathcal{S} of the equation (17), with initial conditions given at $z = z_a$ through the relation

$$\mathbf{H}(z_a, z) = \mathcal{S}(z, z_a)\mathbf{H}(z_a, z_a).$$

With \mathbf{H} and \mathbf{Z} approximated by $\tilde{\mathbf{H}}$ and $\tilde{\mathbf{Z}}$ due to the replacement of r by \tilde{r} according to Eq. (11), the equation for the error $\mathbf{U} = \tilde{\mathbf{H}} - \mathbf{H}$ is

$$\begin{aligned} d\mathbf{U}/dz &= \tilde{\mathbf{H}}\tilde{\mathbf{Z}} - \mathbf{H}\mathbf{Z} = \tilde{\mathbf{H}}\tilde{\mathbf{Z}} + \tilde{\mathbf{H}}\mathbf{Z} - \tilde{\mathbf{H}}\mathbf{Z} - \mathbf{H}\mathbf{Z} = \mathbf{U}\mathbf{Z} + \tilde{\mathbf{H}}(\tilde{\mathbf{Z}} - \mathbf{Z}), \\ \mathbf{U}(z_a, z_a) &= 0, \end{aligned}$$

where Eq. (17) has been used. By *Duhamel's principle* (see e.g. [15, p. 147]), we have that

$$\mathbf{U}(z) = \int_{z_a}^z \mathcal{S}(z, \tau)\tilde{\mathbf{H}}(\tau)(\tilde{\mathbf{Z}}(\tau) - \mathbf{Z}(\tau))d\tau.$$

Since (11) is a linear approximation of $r(z)$, the maximum error in $\tilde{r}(z)$ on $z_a \leq z \leq z + \Delta z$ is of order $\mathcal{O}(\Delta z^2)$. This implies that $\tilde{\mathbf{Z}}$ is also of order $\mathcal{O}(\Delta z^2)$, and

$$\|\mathbf{U}(z_a + \Delta z)\| \leq \Delta z \max_{z_a \leq \tau \leq z + \Delta z} \|\mathcal{S}(z_a + \Delta z, \tau)\tilde{\mathbf{H}}(\tau)(\tilde{\mathbf{Z}}(\tau) - \mathbf{Z}(\tau))\| = \mathcal{O}(\Delta z^3). \quad \blacksquare$$

A consequence of lemma 3.4 is that for segment j in Eq. (5), $\tilde{\mathbf{H}}_j = \mathbf{H}_j + h^3\mathbf{E}_j$ for some $\mathbf{E}_j < \infty$ and a discretisation in segments of length $h = L/N$, where L is the length of the horn.

□

We are now ready to state the convergence theorem for the transmission line model.

THEOREM 3.5. *The transmission line model, with conical segments of length h and planar wavefronts, converges to the transmission matrix found from the solution to the Webster horn equation as the number of segments tends to infinity. Furthermore, the truncation error is of order $\mathcal{O}(h^2)$.*

Proof. For $z_1 \leq z_a \leq z_b \leq z_{N+1}$, let

$$C = \max_{z_a, z_b} \|\mathbf{H}(z_a, z_b)\|.$$

Moreover, let

$$E = \max_{1 \leq j \leq N} \|\mathbf{E}_j\|.$$

For the error $\mathbf{U} = \tilde{\mathbf{H}} - \mathbf{H}$, we have that

$$\begin{aligned} \|\mathbf{U}\| &= \left\| \prod_{j=1}^N (\mathbf{H}_j + h^3 \mathbf{E}_j) - \prod_{j=1}^N \mathbf{H}_j \right\| = \\ &\|\mathbf{H}_1 \mathbf{H}_2 \cdots \mathbf{H}_N + \\ &+ h^3 (\mathbf{E}_1 \mathbf{H}_2 \mathbf{H}_3 \cdots \mathbf{H}_N + \mathbf{H}_1 \mathbf{E}_2 \mathbf{H}_3 \cdots \mathbf{H}_N + \dots + \mathbf{H}_1 \mathbf{H}_2 \cdots \mathbf{H}_{N-1} \mathbf{E}_N) + \\ &+ h^6 (\mathbf{E}_1 \mathbf{E}_2 \mathbf{H}_3 \mathbf{H}_4 \cdots \mathbf{H}_N + \mathbf{E}_1 \mathbf{H}_2 \mathbf{E}_3 \mathbf{H}_4 \cdots \mathbf{H}_N + \\ &\quad + \mathbf{H}_1 \mathbf{E}_2 \mathbf{E}_3 \mathbf{H}_4 \cdots \mathbf{H}_N + \mathbf{H}_1 \mathbf{E}_2 \mathbf{H}_3 \mathbf{E}_4 \mathbf{H}_5 \cdots \mathbf{H}_N + \dots \\ &\quad + \mathbf{H}_1 \mathbf{H}_2 \cdots \mathbf{H}_{N-2} \mathbf{E}_{N-1} \mathbf{E}_N) + \\ &+ h^9 (\mathbf{E}_1 \mathbf{E}_2 \mathbf{E}_3 \mathbf{H}_4 \cdots \mathbf{H}_N + \dots + \mathbf{E}_1 \mathbf{E}_2 \mathbf{H}_3 \mathbf{E}_4 \cdots \mathbf{H}_N + \dots) + \\ &+ \dots + \\ &+ h^{3N} \mathbf{E}_1 \mathbf{E}_2 \cdots \mathbf{E}_N - \mathbf{H}_1 \mathbf{H}_2 \cdots \mathbf{H}_N \|. \end{aligned}$$

By the binomial theorem, we have that

$$\begin{aligned} \|\mathbf{U}\| &\leq h^3 \binom{N}{1} C^2 E + h^6 \binom{N}{2} C^3 E^2 + \dots + h^{3N} \binom{N}{N} C^{N+1} E^N = \\ &= \left(\frac{L}{N}\right)^3 \binom{N}{1} C^2 E + \left(\frac{L}{N}\right)^6 \binom{N}{2} C^3 E^2 + \dots + \left(\frac{L}{N}\right)^{3N} \binom{N}{N} C^{N+1} E^N = \\ &= C \sum_{k=1}^N \left(\frac{L}{N}\right)^{3k} \binom{N}{k} C^k E^k = C \left[\left(1 + \frac{L^3 C E}{N^3}\right)^N - 1 \right]. \end{aligned}$$

Furthermore, it can be shown that there are constants c_1 and c_2 such that

$$\left(1 + \frac{L^3 C E}{N^3}\right)^N - 1 < \frac{c_1}{N^2}, \quad N > c_2,$$

which completes the proof. \blacksquare

3.6. Computation of ∇Z_{in} . The possible design variables of a horn contour as defined by Fig. 2 are the diameters y_1, \dots, y_{N+1} and the segment lengths $z_2 - z_1, \dots, z_{N+1} - z_N$.

An efficient way of computing the gradient of the input impedance Z_{in} with respect to the design variables is necessary for the optimisation algorithm chosen. In some cases, when the function is complicated, the gradient must be approximated using finite differences of the form of the form

$$\frac{\partial Z_{in}}{\partial y_k} \approx \frac{Z_{in}(y_k + \varepsilon) - Z_{in}(y_k)}{\varepsilon}, \quad \varepsilon > 0.$$

This may occasionally be detrimental to the convergence of the optimisation algorithm due to the truncation error in the gradient. However, the preponderant drawback is that the number of function evaluations grows proportionally to the number of design variables. Since the computational cost of each evaluation is also proportional to the number of design variables, the total cost grows as $\mathcal{O}(N^2)$, soon making finite differences infeasible. Fortunately, by symbolic manipulation, and using the appropriate data structures, the gradient of Z_{in} can be computed at a cost corresponding to less than eight times the evaluation cost for Z_{in} , *regardless of the number of segments in the model*.

3.6.1. Gradient with respect to the segment diameters. This section shows how the gradient $\nabla_y Z_L$ with respect to the primitive geometrical variables y_k is computed. The result is used also when other descriptions of the horn contour are used, since the TL method ultimately amounts to a segmental discretisation of the horn. We have

$$\begin{aligned} \frac{\partial Z_{in}}{\partial y_k} &= \frac{\partial}{\partial y_k} \frac{H_{12} + H_{11}Z_L}{H_{22} + H_{21}Z_L} = \\ &= \frac{\frac{\partial}{\partial y_k}(H_{12} + H_{11}Z_L)(H_{22} + H_{21}Z_L) - (H_{12} + H_{11}Z_L)\frac{\partial}{\partial y_k}(H_{22} + H_{21}Z_L)}{(H_{22} + H_{21}Z_L)^2} \\ &= \frac{1}{(H_{22} + H_{21}Z_L)^2} \left[\left(\frac{\partial H_{12}}{\partial y_k} + \frac{\partial H_{11}}{\partial y_k} Z_L + H_{11} \frac{\partial Z_L}{\partial y_k} \right) (H_{22} + H_{21}Z_L) + \right. \\ &\quad \left. - (H_{12} + H_{11}Z_L) \left(\frac{\partial H_{22}}{\partial y_k} + \frac{\partial H_{21}}{\partial y_k} Z_L + H_{21} \frac{\partial Z_L}{\partial y_k} \right) \right]. \end{aligned} \tag{19}$$

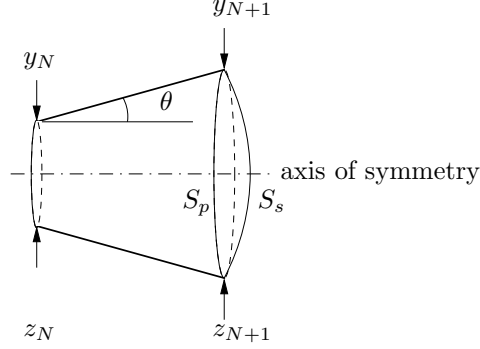
For the computation of $\partial \mathbf{H} / \partial y_k$, define

$$\mathbf{\Pi}_{j,k} = \mathbf{H}_j \mathbf{H}_{j+1} \cdots \mathbf{H}_k, \quad k > j.$$

The only segments that are affected by a change of y_k are those numbered $k-1$ and k . For $3 \leq k \leq N-2$, we may therefore write

$$\begin{aligned} \frac{\partial \mathbf{H}}{\partial y_k} &= \frac{\partial}{\partial y_k} (\mathbf{\Pi}_{1,k-2} \mathbf{H}_{k-1} \mathbf{H}_k \mathbf{\Pi}_{k+1,N}) = \\ &= \mathbf{\Pi}_{1,k-2} \left(\frac{\partial \mathbf{H}_{k-1}}{\partial y_k} \mathbf{H}_k + \mathbf{H}_{k-1} \frac{\partial \mathbf{H}_k}{\partial y_k} \right) \mathbf{\Pi}_{k+1,N}. \end{aligned} \tag{20}$$

The cases $k = 1, 2, N, N+1$ are dealt with correspondingly. Computing $\mathbf{\Pi}_{1,1}, \mathbf{\Pi}_{1,2}, \dots, \mathbf{\Pi}_{1,N-1}$, and $\mathbf{\Pi}_{N,N}, \mathbf{\Pi}_{N-1,N}, \dots, \mathbf{\Pi}_{2,N}$ requires a total of $2N-3$ matrix multiplications, if all the intermediate results are stored. The computer implementation of the gradient computation thus utilises two three-dimensional arrays that contain all the necessary cumulative products involved in (20) for $k = 1, \dots, N$.

FIG. 4. *The rightmost segment.*

The derivatives of \mathbf{H}_j with respect to their end diameters can either be approximated by finite differences, or obtained symbolically. The symbolic results become quite wieldy due to the already somewhat involved expressions for the \mathbf{H}_j :s, and are therefore presented in Appendix. As an alternative to symbolic differentiation of \mathbf{H}_j , centred second-order finite-difference approximations can be used. The computational cost of this is in fact somewhat lower than if the corresponding exact expressions are used. Experimentally, the finite-difference approximations did not appear to introduce any problems for the optimisation routine, although one should be aware of the importance of accuracy in the gradient for optimisation problems.

The radiation impedance of an un-flanged cylindrical pipe of radius a according to Beranek [6] is given by

$$Z_{L0} = 0.25 \frac{\omega^2 \rho}{\pi c} + i 0.6133 \frac{\rho \omega}{\pi a}. \quad (21)$$

To the author's knowledge, no corresponding approximation of the radiation impedance at the end of a cone has been derived, but a reasonable modification of (21) is (cf. [11])

$$Z_L = Z_{L0} \frac{S_p}{S_s},$$

where S_p is the cross-sectional area of the cylinder, and S_s the spherical wave front area at the open end of the cone. The area S_s of a spherical cap is given by $S_s = 2S_p/(1 + \cos \theta)$, with notations according to Fig. 4. This gives

$$Z_L = Z_{L0} \frac{1 + \cos \theta}{2} = Z_{L0} \left(\frac{1}{2} + \frac{\ell_1}{2\gamma} \right),$$

where $\ell_1 = z_{N+1} - z_N$ and $\gamma = \sqrt{\ell_1^2 + \ell_2^2}$, $\ell_2 = (y_{N+1} - y_N)/2$. For $\partial Z_L / \partial y_N$

we thus have

$$\begin{aligned}
\frac{\partial Z_L}{\partial y_N} &= Z_{L0} \frac{\partial}{\partial y_N} \frac{\ell_1}{2\gamma} = Z_{L0} \left(\frac{-\ell_1}{2\gamma^2} \right) \frac{\partial \gamma}{\partial y_N} = \\
&= Z_{L0} \left(\frac{-\ell_1}{2\gamma^2} \right) \frac{1}{2\sqrt{\ell_1^2 + \left(\frac{y_{N+1} - y_N}{2} \right)^2}} \left(-\frac{y_{N+1} - y_N}{2} \right) = \\
&= Z_{L0} \frac{\ell_1}{8\gamma^3} (y_{N+1} - y_N) = Z_{L0} \frac{\ell_1 \ell_2}{4\gamma^3}.
\end{aligned} \tag{22}$$

The expression for $\partial Z_L / \partial y_{N+1}$ is derived similarly using $a = y_{N+1}/2$ in (21),

$$\begin{aligned}
\frac{\partial Z_L}{\partial y_{N+1}} &= \frac{\partial Z_{L0}}{\partial y_{N+1}} \left(\frac{1}{2} + \frac{\ell_1}{2\gamma} \right) + Z_{L0} \frac{\partial}{\partial y_{N+1}} \frac{\ell_1}{2\gamma} = \\
&- i0.6133 \frac{2\rho\omega}{\pi y_{N+1}^2} \left(\frac{1}{2} + \frac{\ell_1}{2\gamma} \right) - Z_{L0} \frac{\ell_1 \ell_2}{4\gamma^3}.
\end{aligned} \tag{23}$$

Using equations (19), (20), (22) and (23), each component of $\nabla_y Z_{in}$ can be evaluated.

3.6.2. Gradient with respect to segment lengths. The gradient with respect to the lengths of the conical segments is computed in the same way as in the previous section.

4. Finding smooth solutions.

4.1. Optimisation with respect to the segment diameters.

4.1.1. Theory. As a first application of the optimisation, (3) was minimised with y_k , $k = 2, \dots, N$ as design variables. The profile was tied in at the end points by keeping y_1 and y_{N+1} fixed. The segment lengths $z_2 - z_1, \dots, z_{N+1} - z_N$ were also held fixed.

Geometrically, designs for which $y_k \leq 0$ do not make sense. The inequality bound $y_k > 0$ can therefore be imposed without eliminating any meaningful part of the design space. Nevertheless, this constraint was not imposed on the problem, mainly because the optimisation routine chosen does not handle bound constraints.

4.1.2. Experiments. As a model problem, a Bessel horn of length 0.5 m (Fig. 7) was chosen as subject to intonation optimisation.

The aim was to lower the frequencies of the three first impedance peaks by 10 Hz. The throat and end diameters y_1 and y_{N+1} were held fixed, whereas all interior segment diameters are free parameters. For this problem, the non-linear least squares routine `lsqnonlin` of the Optimization Toolbox of MATLAB was used. The termination tolerance of the design variables was set to 10^{-6} , which yields designs of an accuracy well beyond what can be machined, should the horn be constructed in practice. The same tolerance was used also for all subsequent

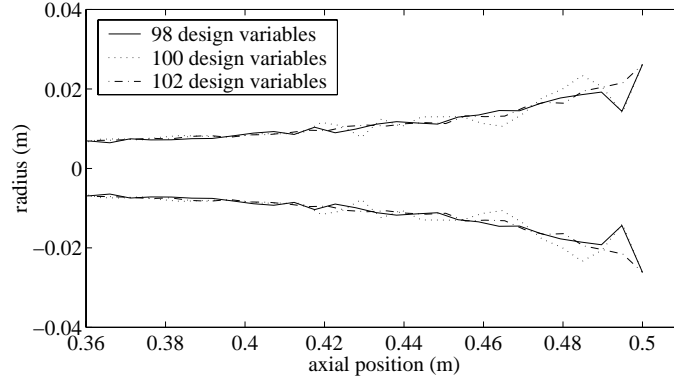


FIG. 5. *The results for a 10 Hz peak placement computed for three choices of discretisation.*

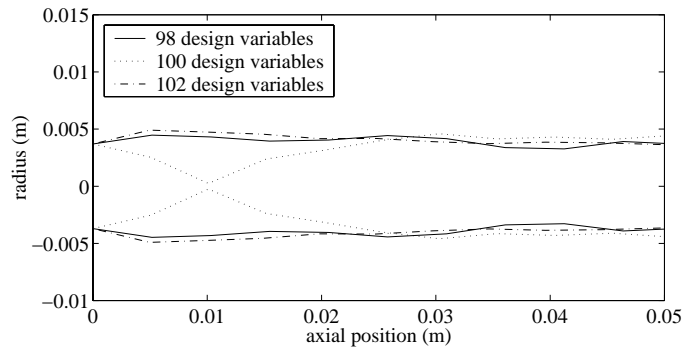


FIG. 6. *The “lead pipes”.*

optimisation tasks. The Figs. 5 and 6 show the bell shapes obtained with three slightly different choices of discretisations.

Even if the optimisation converges, it is not certain that the obtained design is feasible in practice. A problem common to many applications of shape optimisation is the tendency for the development of irregular or ragged shapes. Even if the physical model is still valid for non-smooth shapes – something that is certainly not always the case – such shapes may be unsatisfactory for structural or productional reasons, not to mention their visual appearance. Although the numbers of transmission line elements are almost the same, the results vary vastly. None of the solutions is particularly attractive with their sawtooth-like appearances, jagged to the extent that the validity of the transmission line model is questionable. One might ask if it is possible to get rid of the oscillations by refining the discretisation. Unfortunately, doubling the number of conical segments in the model does not seem to help matters much, as can be seen from

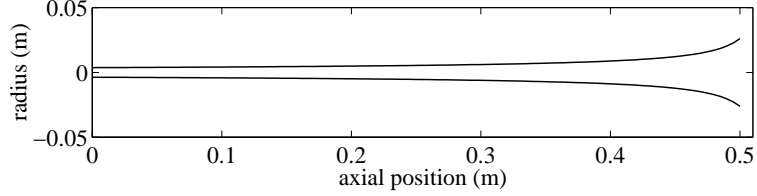
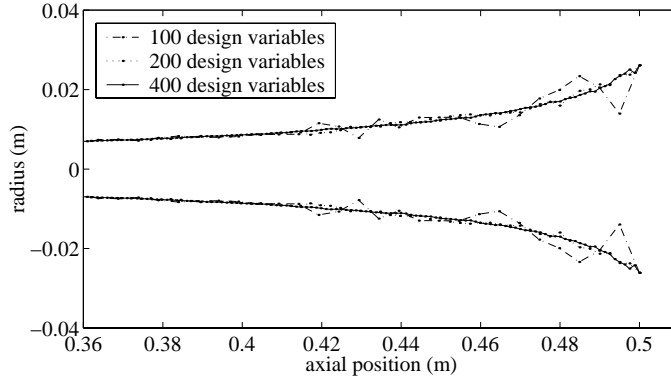
FIG. 7. *Bessel horn used as a test example.*

Fig. 8. Refining the discretisation to 400 design variables gives a somewhat smoother design, but some fine scaled ripple remains.

FIG. 8. *Intonation experiment with three different discretisations.*

An even more severe problem shows if, for instance, an attempt is made to move the peaks as above, but by 20 Hz. This makes the horn profile break down completely, and the optimisation algorithm diverges. Conclusively, optimising directly with respect to the cone segment diameters is not a viable way to design horns.

4.2. Regularisation. A common way to remedy the problem with non-smooth solutions, and in particular to provide existence of solutions to ill-posed problems, is to use so-called *Tikhonov regularisation* [28]. This is a way of enforcing smoothness by introducing a penalty term in the objective function. One choice is to define

$$J^\epsilon(\alpha) = J(\alpha) + \frac{\epsilon}{2} \int \eta^2 dz, \quad (24)$$

where

$$\eta = y''.$$

y'' is roughly a measure of the curvature of y , and through the choice of ϵ , arbitrarily smooth solutions can be obtained.

There are two drawbacks to Tikhonov regularisation. The first one is the difficulty in selecting a suitable value of ϵ . It is hard to give any precise guidelines for this, so the choice will have to be subject to experimentation with the problem at hand. The second disadvantage is that the objective function (24) defines an optimisation problem where intonation quality is, to some extent, traded for smoothness of the horn. This is clearly not preferable for intonation tasks. For these reasons, the Tikhonov approach is therefore not perused any further in this paper.

4.3. Constraining the search space.

4.3.1. Theory. Another way of achieving smooth solutions is to reduce the search space to include only designs that are geometrically acceptable. This can be done explicitly, by imposing constraints on the design variables, or implicitly, by parametrising the design boundary by some appropriate function. A brass instrument bell might for instance be designed by determining the coefficients in the expression for a Bessel horn [4],

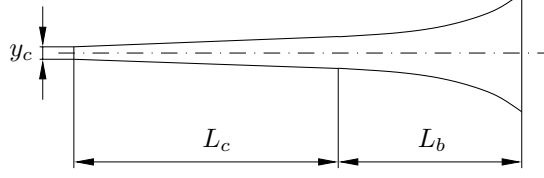
$$y(z) = \frac{B}{(D_0 - z)^m}, \quad (25)$$

a shape which describes many classical horns rather well. However, if the number of degrees of freedom is too small, it might not be possible to obtain anything but sub-optimal solutions. A more flexible approach would be to let the horn shape be described by a number of control points, between which the horn contour is obtained by spline interpolation. Obviously, if the number of control points is moderate, wiggly contours cannot even be represented. On the other hand, if the number of control points is increased, oscillations may appear also for a spline representation.

Nevertheless, the sub-optimal solutions may be useful as a starting point for further fine intonation with a larger number of degrees of freedom. Consider a geometry defined by the parameters $\alpha = (\alpha_1, \alpha_2, \dots, \alpha_m)^T$. The horn is as before discretised using N conical elements. By the chain rule,

$$\frac{\partial Z_{in}}{\partial \alpha_k} = \sum_{j=1}^N \frac{\partial Z_{in}}{\partial y_j} \frac{\partial y_j}{\partial \alpha_k}. \quad (26)$$

Instead of formulating the objective function from observations of Z_{in} at fixed frequencies, as in (1), it is possible to define an objective function that includes the actual *deviations* of the zeros of $\text{Im}(Z_{in})$. This will also increase the convergence radius of the optimisation greatly, since there is no ambiguity in the identification of the zeros. Although generalisations are possible, we will look at an example that only includes the zero shifts, but excludes the peak impedance

FIG. 9. *Parametrised horn.*

values. For a restricted geometrical description, this is possible in spite of the general need for magnitude specification, as discussed in 2.1.

The computation of the objective function and its gradient is done in the following way²;

1. Find the zeros φ_k , $k = 1, \dots, n$ of $\text{Im}(Z_{in}(f))$
2. Form \mathbf{F} , $F_k = f_{\text{peak}_k} - \varphi_k$.
3. Form $\partial F_k / \partial \alpha_j = \frac{\text{Im}(\partial Z_{in}(\varphi_k) / \partial \alpha_j)}{\text{Im}(\partial Z_{in}(\varphi_k) / \partial f)}$.

Step 3 follows from differentiation of

$$\text{Im}(Z_{in}(\varphi_k(\boldsymbol{\alpha}); \boldsymbol{\alpha})) \equiv 0$$

with respect to α_j , which gives

$$\text{Im} \left(\frac{\partial Z_{in}(\varphi; \boldsymbol{\alpha})}{\partial f} \frac{\partial \varphi_k}{\partial \alpha_j} \right) + \text{Im} \left(\frac{\partial Z_{in}(\varphi; \boldsymbol{\alpha})}{\partial \alpha_j} \right) = 0$$

or

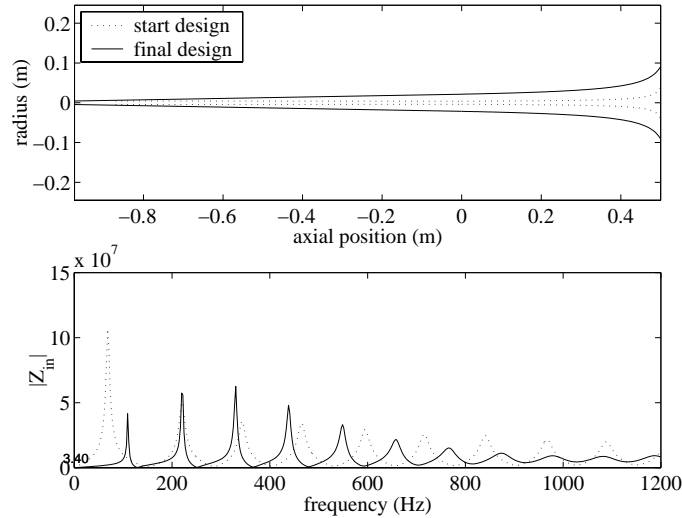
$$\frac{\partial \varphi}{\partial \alpha_j} = - \frac{\text{Im}(\partial Z_{in}(\varphi) / \partial \alpha_j)}{\text{Im}(\partial Z_{in}(\varphi) / \partial f)}.$$

In practice, step 1 has to be carried out in a way that automatically finds the n first zeros. In this work, the zeros of a piece-wise quadratic interpolant for a sampling of $\text{Im}(Z_{in})$ were used to find initial guesses for a scalar secant root finding algorithm. The roots corresponding to impedance minima were excluded by comparison with an interpolant based maximum finder applied on $\text{Re}(Z_{in})$.

We also see that it is now necessary to differentiate Z_{in} with respect to the frequency f . If need be, this is done analytically along the lines of section 3.6.1, using the chain rule. A computationally somewhat less expensive, and accurate enough, alternative is again to use a finite-difference approximation.

The process of finding the roots of $\text{Im}(Z_{in})$ is computationally more involved than merely evaluating Z_{in} at the desired peak frequencies, but the extra cost is justified for this more general design approach.

²In the following, f_{peak} refers to a zero of $\text{Im}(Z_{in})$ although, as mentioned, the zeros are not exactly equal to the locations of the impedance peaks

FIG. 10. *Harmonic instrument constructed of a cone and a Bessel horn.*

4.3.2. Experiments. The following example shows how a parametrised description can be used for the design of an instrument with prescribed resonance frequencies. Consider the instrument shown in Fig. 9. A bell defined by equation (25) (dimensions in m) is attached to a conical pipe of length L_c . The length L_b of the bell and the left end diameter y_c of the conical pipe are fixed; all other dimensions are given by L_c , B , D_0 and m . Since L_c is a free parameter, one of the terms in (26) involves the differentiation of Z_{in} with respect to the first segment of the model.

The aim was to design a harmonic horn in A natural, with the first eight impedance peaks at integer multiples of 110 Hz. The two fixed dimensions were chosen as $L_b = 500$ mm and $y_c = 9$ mm – in the range of what can be expected for an instrument in the register at hand. The start design, given by $L_c = 870$ mm, $B = 5$ mm, $D_0 = 510$ mm and $m = 0.6$ is indicated in Fig. 10. After 98 iterations, the gradient had dropped 13 decades and curiously, considering that the problem has only four degrees of freedom, a solution was obtained for which none of the first eight fundamentals is off by more than 0.45%, or eight musical cents. Not surprisingly however, the resulting horn brings in mind the Flügelhorn, an instrument with an intonated fundamental.

In a second example, the second through eighth overtones were kept in place, but the fundamental was placed at 80 Hz. This arrangement mimics the conditions of eg. the trumpet. Convergence was this time reached in ten iterations. The trumpet-like result, with its nearly cylindrical main tubing shown in Fig. 11, is again not surprising.

Information about the residual and gradient norm decrease for the two cases

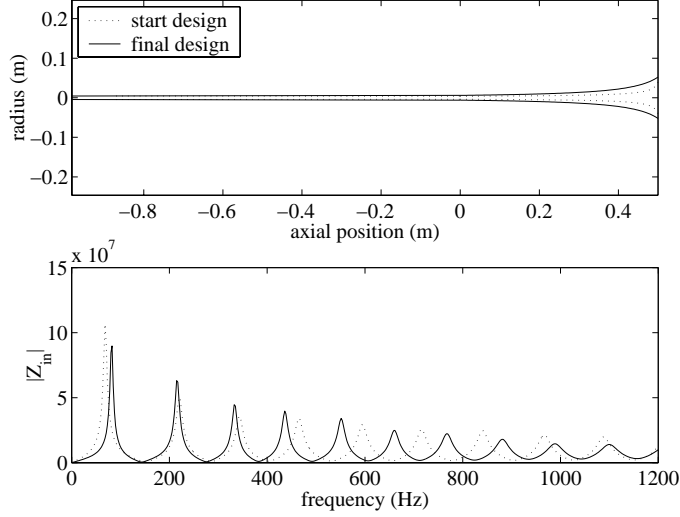


FIG. 11. Instrument with a “displaced fundamental”.

is shown in Fig. 12. As can be seen, convergence is roughly linear in both cases. For the harmonic horn, however, the convergence rate is slower and the optimiser did not manage to take full steps throughout the process. It is not clear why superlinear convergence cannot be detected in any of the two cases. Possible explanations are the influence of rounding errors, or simply that the region of superlinear convergence is so small that the solution has converged within tolerance before the superlinear region is reached.

4.4. Smoothing. A desirable feature would be if we could somehow retain the size of the design space, but give the optimisation process a *preference* to search for smooth solutions. This can be accomplished by the use of *smoothing*. The application of this technique to an acoustic shape optimisation problem has been described in detail in [3], but a condensed description of the principles and merits of smoothing is given here.

4.4.1. Theory. The basic idea behind smoothing is to introduce a design variable transformation that, considering each design as a point in a multi- or infinitely-dimensional space, implicitly “moves” irregular or ragged designs, associated to unwanted local minima, away from smooth designs, but without actually excluding any part of the search space. The principle is to introduce the following change of variables,

$$\begin{cases} y''(z) &= \eta, & z \in [0, a] \\ y(0) &= y_0 \\ y(a) &= y_a, \end{cases} \quad (27)$$

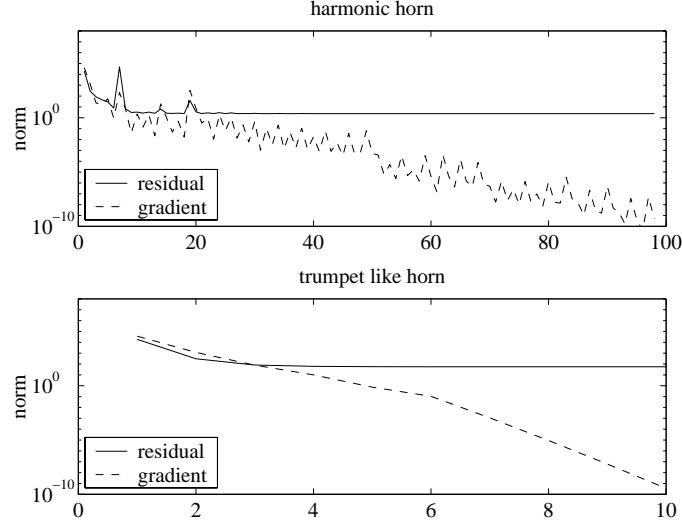


FIG. 12. Residual and norm of gradient as a function of the iteration count.

and then optimise with respect to η . This transformation ties in the end point values of y , as was the case in the formulation of the optimisation problem in Sec. 4.1, but variations are possible. Eq. (27) defines an isomorphism between η and y , which formally implies

$$\frac{\partial J}{\partial \eta} = \frac{\partial J}{\partial y} \frac{\partial y}{\partial \eta},$$

by the chain rule. (In the continuous case, the derivatives should be interpreted in the *Frechet* sense, but further discussions on this matter are left out in this paper). The isomorphism guarantees that $\partial y / \partial \eta$ is non-singular, and a minimum of $\partial J / \partial \eta$ will also be a minimum of $\partial J / \partial y$. Thus, the change of variables preserves optimal solutions.

Each step of the Levenberg-Marquardt method can be interpreted as a weighted combination of a Gauss-Newton step, and a steepest descent step. The choice of the weighting is based on a trust-region approach, where the optimiser compares the decrease in the objective function to a predicted

For a Newton method, a change of variables essentially does not affect the convergence near a minimum. Intuitively, Newton's method can be thought of as choosing the metric of the search space in a manner that transforms oblong or oval valleys in the objective function to circular pits. The step-length taken in the direction towards the minimum is automatically adjusted in a way that yields quadratic convergence. Any previous variable change, such as (27), that distorts the shape of a minimum is therefore intrinsically “undone” by Newton's method. However, for the steepest descent method, the change of variables does

have an effect on the path the optimisation takes in the search space. An intuitive interpretation of how the smoothing works together with a steepest descent-type optimisation algorithm is that the physical variable y is always smoother than η , the variable with respect to which the optimisation is done [3].

For a Newton method, this does not really affect the convergence near a minimum. Intuitively, Newton's method can be thought of as change of the metric of the search space in a manner that transforms oblong or oval valleys in the objective function to circular pits. The step-length taken in the direction towards the minimum is automatically adjusted in a way that yields super-linear convergence. Any previous variable change, such as (27), that distorts the shape of a minimum is therefore intrinsically “undone” by Newton's method. However, the super-linear convergence of Newton's method is valid only sufficiently near a minimum. Farther away from it, the method is unpredictable and might fail to converge. This problem is usually remedied by using a more robust search method as long as the iterates are estimated to be outside some trust region. In the Levenberg-Marquardt algorithm used here, a conjugate-gradient method combined with cubic line search is used outside the trust region. Here is where the change of variables does have an effect on the path the optimisation takes in the search space. An intuitive interpretation of how the smoothing works together with a steepest descent-type optimisation algorithm is that the physical variable $y(z)$ is always smoother than η , the variable with respect to which the optimisation is done [3].

It should be noted that the advocated method of optimising with respect to the right hand side of a one-dimensional Poisson type equation is not restricted to the gradient based optimisation method used in this work. Other methods that have the property that convergence to a solution near the initial design is more likely than convergence to more distant solutions, may benefit from this approach. The interpretations of “near” and “distant” would depend on the chosen method, though.

4.4.2. Discrete approximation of the smoothing equation. Equation (27) has to be discretised in order for it to be applicable as a variable transformation for the discrete TL-model. One possibility is to make a 1-D finite-element formulation (FEM) of the equation, using the standard nodal based piece-wise linear “hat”-functions [27, p. 27]. y and η are then approximated by the expansions

$$y_h(z) = \sum_{j=1}^{N+1} y_j w_j \quad \text{and} \quad \eta_h(z) = \sum_{j=1}^{N+1} \eta_j w_j.$$

A variational formulation of (27) is

$$\int_0^a y''(z)v(z) \, dz = \int_0^a \eta(z)v(z) \, dz \quad \forall v \in H^1$$

or

$$y'(a)v(a) - y'(0)v(0) - \int_0^a y'(z)v'(z) dz = \int_0^a \eta(z)v(z) dz.$$

The finite-element approximation of this equation is defined for those test functions whose support is in $[0, a]$. We have

$$\begin{aligned} - \sum_{j=1}^{N+1} y_j \int_0^a w'_j(z)w'_i(z) dz &= \\ &= \sum_{j=1}^{N+1} \eta_j \int_0^a w_j(z)w_i(z) dz \quad \forall w_i, i = 2, \dots, N, \end{aligned} \quad (28)$$

which constitutes $N - 1$ equations for the $N + 1$ unknown y_j :s. The simplest way to handle the essential boundary conditions is to insert the nodal values at the boundaries into the systems of equations as shown below. The inner products between the basis functions and their derivatives in (28) are

$$\begin{aligned} \int_0^a w'_i w'_{i-1} dz &= -\frac{1}{h_i}, \\ \int_0^a w'_i w'_i dz &= \frac{1}{h_i} + \frac{1}{h_{i+1}}, \\ \int_0^a w'_{i+1} w'_i dz &= -\frac{1}{h_{i+1}}, \\ \int_0^a w_i w_{i-1} dz &= \frac{1}{6} h_i, \\ \int_0^a w_i w_i dz &= \frac{1}{3} (h_i + h_{i+1}) \\ \int_0^a w_{i+1} w_i dz &= \frac{1}{6} h_{i+1}, \end{aligned}$$

where $h_i = z_{i+1} - z_i$. On matrix form, (28) together with the boundary conditions, can be written

$$\mathbf{K}\mathbf{y} = \mathbf{M}\boldsymbol{\eta} + \mathbf{b} \Leftrightarrow \mathbf{y} = \mathbf{K}^{-1}(\mathbf{M}\boldsymbol{\eta} + \mathbf{b}),$$

where

$$\mathbf{K} = \begin{bmatrix} 1 & 0 & 0 & \cdots & \cdots & 0 \\ \frac{1}{h_1} & -\frac{1}{h_1} - \frac{1}{h_2} & \frac{1}{h_2} & 0 & \cdots & 0 \\ 0 & \frac{1}{h_2} & -\frac{1}{h_2} - \frac{1}{h_3} & \frac{1}{h_3} & 0 & 0 \\ \vdots & & & \ddots & & \vdots \\ 0 & \cdots & \cdots & 0 & \frac{1}{h_{N-1}} & -\frac{1}{h_{N-1}} - \frac{1}{h_N} & \frac{1}{h_N} \\ 0 & \cdots & & \cdots & 0 & 0 & 1 \end{bmatrix},$$

$$\mathbf{M} = \begin{bmatrix} 0 & 0 & \cdots & \cdots & 0 \\ \frac{h_1}{6} & \frac{h_1+h_2}{3} & \frac{h_2}{6} & 0 & \cdots & 0 \\ 0 & \frac{h_2}{6} & \frac{h_2+h_3}{3} & \frac{h_3}{6} & 0 & \cdots & 0 \\ \vdots & & & \ddots & & \ddots & \vdots \\ 0 & \cdots & & 0 & \frac{h_{N-1}}{6} & \frac{h_{N-1}+h_N}{3} & \frac{h_N}{6} \\ 0 & 0 & \cdots & & \cdots & \cdots & 0 \end{bmatrix}$$

and

$$\mathbf{b} = (y_0, 0, \dots, 0, y_a)^T.$$

Furthermore

$$\frac{d\mathbf{y}}{d\boldsymbol{\eta}} = \mathbf{K}^{-1}\mathbf{M},$$

which is used in the discrete relation

$$\frac{\partial J}{\partial \boldsymbol{\eta}} = \left(\frac{\partial \mathbf{y}}{\partial \boldsymbol{\eta}} \right)^T \frac{\partial J}{\partial \mathbf{y}}.$$

The FEM was chosen due to its flexibility to deal with discretisations of non-constant step sizes h_j . A finite-difference approximation would also be a possible choice. It should be noted that a small discretisation error in the approximation of (27) is not crucial. The important property of the change of variables is that it essentially represents a low pass filtering when going from η to y .

4.4.3. Experiments. The results of this section refer to optimisation problems with the objective function (2). The experiment of section 4.1 was repeated with the smoothing applied. The segment lengths were kept constant. Fig. 13

shows the resulting bell shapes for 100, 200 and 400 conical sections. Convergence to a result for which J vanishes within tolerance was achieved in 21, 20 and 20 iterations, respectively. Apparently, the problem with jagged solutions has been cured efficiently. It is however not possible to detect convergence to some specific shape as the number of discretisation points (and also the number of design variables) is increased. Uniqueness is not to be expected either, since the design variables out-number the residuals of the least squares problem with more than one order of magnitude.

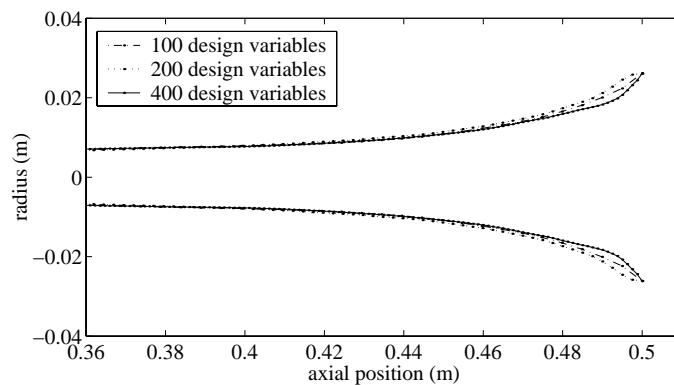


FIG. 13. *Intonation experiment with three different discretisations and smoothing applied.*

4.5. A continuation method. Large deformations are required if the properties of the target design are very different from those of the original design. Gradient based optimisation algorithms often run into problems in such cases. The iteration may get stuck in a local minimum, converge to a solution that is geometrically unacceptable, or simply fail to converge at all. Gradient free optimisation strategies, such as genetic algorithms or the Rosenbrock method, have been employed successfully [17], and although they converge very slowly, they are quite robust. However, gradient based algorithms can be used also for quite difficult design problems using a *continuation* method. The idea is to gradually change the target properties so that the deformation of each optimisation step is sufficiently small. One method that was tried for the impedance placement–peak level task presented in table 1 was to successively evolve the target properties from those of the start design, to the properties of the desired design. Define

$$\mathcal{Z} = \begin{bmatrix} f_{\text{peak}_1} & Z_{\text{peak}_1} \\ f_{\text{peak}_2} & Z_{\text{peak}_2} \\ \vdots & \vdots \\ f_{\text{peak}_n} & Z_{\text{peak}_n} \end{bmatrix},$$

a matrix with the impedance peak frequencies in the first column, and the corresponding levels in the second column. The optimisation can then be performed in N_{cont} steps, in each of which the target property \mathcal{Z}_j is given by

$$\mathcal{Z}_j = (1 - s)\mathcal{Z}_{\text{start}} + s\mathcal{Z}_{\text{target}},$$

where $s = j/N_{\text{cont}}$. This approach is called the *gradual continuation method*. Results from the task in table 1 with $N_{\text{cont}} = 8$ are presented in Fig. 14 and 15, where the intermediate results refer to the case $j = 4$. The method of gradual continuation was again run, but in only two steps. The results from this run are shown in Fig. 16 and 17.

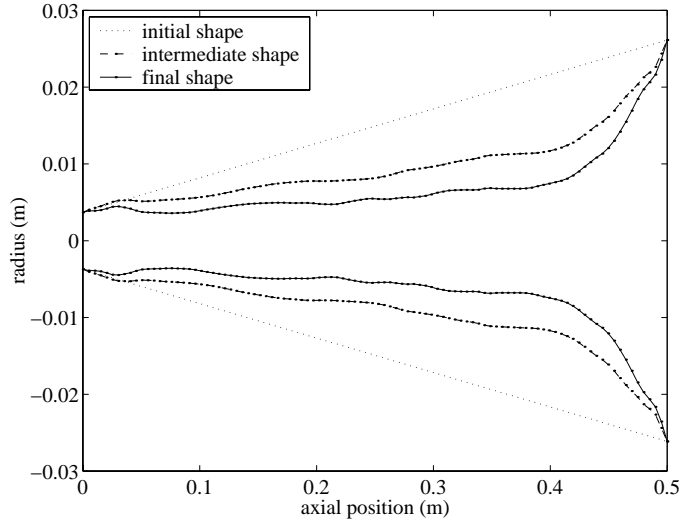


FIG. 14. *Horn geometry from an eight step gradual continuation optimisation. Frequencies and magnitudes of the three first impedance peaks were considered.*

A related method is to place the peaks at the desired locations, and *then* adjust the levels. Results of such a two step process, called the *two-pass location-level method*, are presented in the Fig. 18 and 19.

The experiments suggest that the continuation methods is capable of “guiding the optimisation in the right direction”, but a large number of continuation steps *per se* is not necessarily advantageous to the final result. A gradual change in too many steps seems to somehow preclude the optimisation from finding its way to a smooth solution.

In order to test the properties of the optimisation algorithm, along with the two different continuation approaches, a slightly more challenging problem was formulated. The idea was to try to reproduce the locations and magnitudes of the first nine impedance peaks of a 0.5 m long Bessel horn, as given by Eq. (25). The

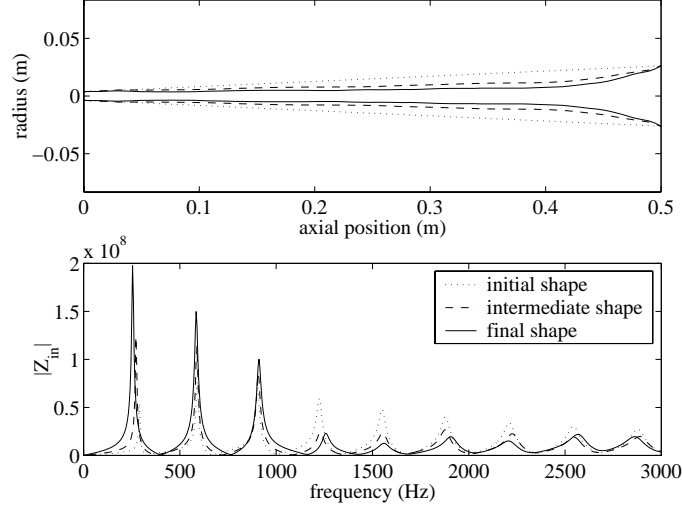


FIG. 15. Results from an eight step gradual continuation optimisation. Frequencies and magnitudes of the three first impedance peaks were considered.

constants in the representation were $B = 0.005$, $m = 0.6$ and $D_0 = 0.52$. With 100 conical elements, the transmission line model yielded the peak locations and magnitudes shown in the right column of table 3. The initial geometry was a cone with the same end diameters as the Bessel horn.

Figs. 20 and 21 show the results obtained with the two-pass location-level method, and a two step gradual continuation method. Here it becomes even more apparent that the separation between peak-placement and level-adjustment seems to yield smoother designs than when both these tasks are dealt with simultaneously, even for small design steps in the continuation method.

Figs. 22 and 23 show the shape and the impedance spectrum of the horn reconstructed with the two-pass location-level method. Although some minute oscillations in the design are noticeable, the result agrees well with the original horn profile.

The residual and gradient norms for the location-level experiment are shown in Fig. 24. The curves indicate that J converges superlinearly to zero. The better convergence property shown in Fig. 24 when compared to Fig. 12 can be explained by the fact that the former problem is under determined, whereas the latter problem is over determined.

4.6. Smoothness optimisation. The last example of how ∇Z_{in} can be used for gradient based optimisation is somewhat different from the previous ones. The purpose of those was to find designs that satisfied certain intonation properties. In this section, the aim is to minimise the oscillations of a horn that already satisfies the intonation goal.

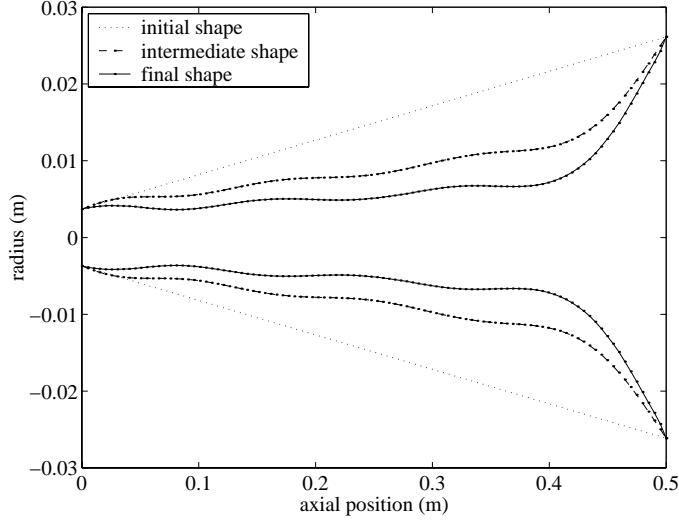


FIG. 16. *Horn geometry from a two step gradual continuation optimisation. Frequencies and magnitudes of the three first impedance peaks were considered.*

A measure of the variation of a horn profile is defined by

$$j(\boldsymbol{\eta}) = \int_0^a (\beta(z)y''(z))^2 dz = \int_0^a \beta^2(z)\eta^2(z) dz, \quad (29)$$

where $\beta(z)$ is a weighting function chosen to enforce regularity in different parts of the horn. If no deviation in the desired intonation objective is tolerated, our new design problem takes the form of an equality constrained non-linear least squares problem,

$$\boldsymbol{\eta}^* = \arg \min_{\boldsymbol{\eta}} j(\boldsymbol{\eta}) \quad \text{subject to} \quad \mathbf{g}(\boldsymbol{\eta}) = \mathbf{0}, \quad (30)$$

where $\mathbf{g}(\boldsymbol{\eta})$ is actually identical to (3). If the problem lacks a feasible solution, that is a solution such that $\mathbf{g}(\boldsymbol{\eta}) = \mathbf{0}$, an inequality constraint must be used instead. Most algorithms for non-linear constrained optimisation use *sequential quadratic programming* (SQP). The function `fmincon` of the Optimisation toolbox of MATLAB is one such method. The objective function (29) is of course very well suited for SQP, but the nonlinear constraint is costly to compute.

As a test case for the smoothness optimisation, a shape obtained in a profile reconstruction experiment like in section 4.5 was investigated. The reconstruction was made from only six peaks in order to emphasise the wiggles. It should again be emphasised that this is not an inverse problem. The test case is suitable however, since we know that there is a smooth solution to the design problem. As can be seen from Fig. 25, the slightly wiggly initial design was smoothed

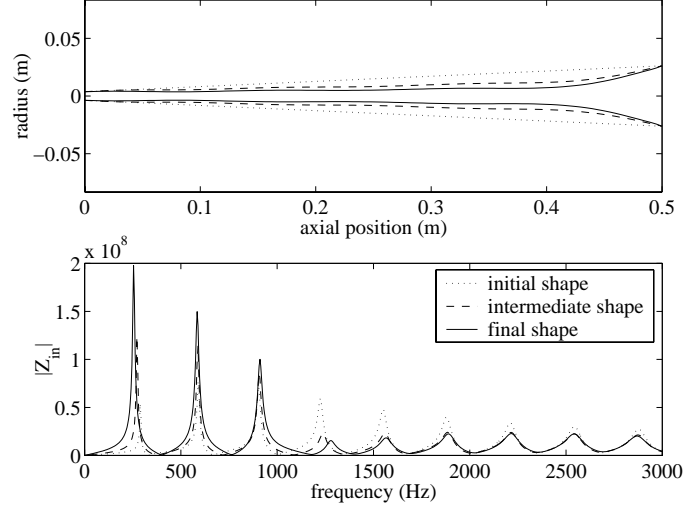


FIG. 17. Results from a two step gradual continuation optimisation. Frequencies and magnitudes of the three first impedance peaks were considered.

considerably, if not completely. The convergence criterion of the optimisation routine was sharp enough to guarantee that the remaining wiggles correspond to a local solution. Although the objective function is certainly convex, the constraints are not. This fact makes it difficult to find the global solution of the problem.

start impedance		goal impedance	
location (Hz)	magnitude (Ω)	location (Hz)	magnitude (Ω)
290.3	$6.5 \cdot 10^7$	255	$2.0 \cdot 10^8$
591.3	$8.0 \cdot 10^7$	585	$1.5 \cdot 10^8$
904.4	$7.2 \cdot 10^7$	910	$1.0 \cdot 10^8$

TABLE 1

Start and goal properties for an intonation experiment.

start impedance		intermediate impedance		goal impedance	
loc. (Hz)	mag. (Ω)	loc. (Hz)	mag. (Ω)	loc. (Hz)	mag. (Ω)
290.3	$6.5 \cdot 10^7$	255	$6.5 \cdot 10^7$	255	$2.0 \cdot 10^8$
591.3	$8.0 \cdot 10^7$	585	$8.0 \cdot 10^7$	585	$1.5 \cdot 10^8$
904.4	$7.2 \cdot 10^7$	910	$7.2 \cdot 10^7$	910	$1.0 \cdot 10^8$

TABLE 2

Start and goal properties for a two-step intonation experiment.

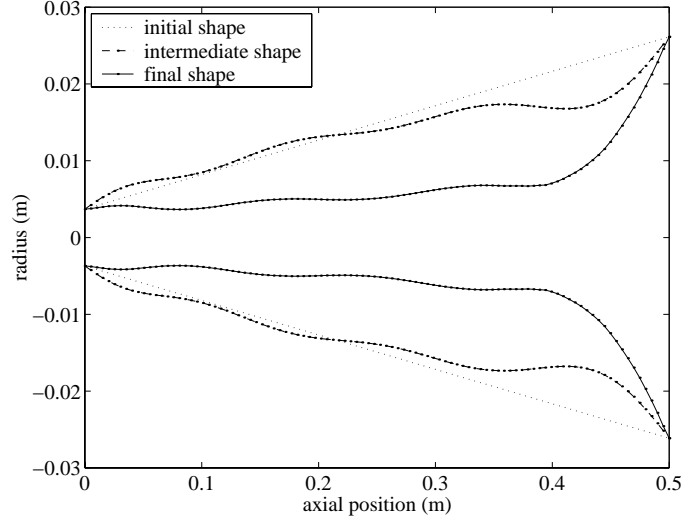


FIG. 18. *Horn geometry from a two-pass location-level optimisation. Frequencies and magnitudes of the three first impedance peaks were considered.*

start impedance		goal impedance	
location (Hz)	magnitude (Ω)	location (Hz)	magnitude (Ω)
290.3	$6.5 \cdot 10^7$	266.5	$2.0 \cdot 10^8$
591.3	$8.0 \cdot 10^7$	594.0	$1.4 \cdot 10^8$
904.4	$7.2 \cdot 10^7$	921.8	$9.5 \cdot 10^7$
1226	$5.9 \cdot 10^7$	1249	$6.6 \cdot 10^7$
1553	$4.8 \cdot 10^7$	1574	$4.6 \cdot 10^7$
1883	$4.0 \cdot 10^7$	1900	$3.3 \cdot 10^7$
2215	$3.4 \cdot 10^7$	2225	$2.5 \cdot 10^7$
2549	$3.0 \cdot 10^7$	2550	$2.1 \cdot 10^7$
2883	$2.7 \cdot 10^7$	2874	$1.8 \cdot 10^7$

TABLE 3

Start and goal properties for an intonation experiment with nine peaks (figures with 15 decimal places were used in practice).

5. Computational performance. All the computer code that was used in this project was written in MATLAB. The Levenberg-Marquardt routine is part of the Optimization Toolbox. A typical intonation experiment takes a few minutes on a 450MHz UltraSPARC-II, but since MATLAB is an interpreting language, these figures are not representative of the performance of a productional version of the code. A compiled version written in `fortran90` or `C`, for instance, would run considerably faster. There may also be room for optimisation of the code. At present, computing the input impedance *and* its gradient

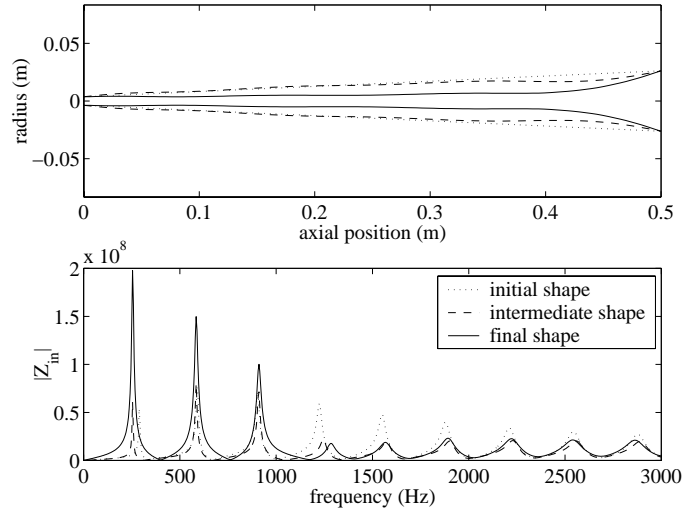


FIG. 19. *Horn geometry from a two-pass location-level optimisation. Frequencies and magnitudes of the three first impedance peaks were considered.*

requires around 7.4 times the number of floating point operations as compared to computing the input impedance alone with a designated and efficient code. This figure can probably be improved somewhat, although not substantially.

To this date, there is no design tool for wind instruments that works completely without human interaction. With all acoustical, musical and architectural considerations that come into play in the design of an instrument, it is therefore necessary that the design algorithm works rapidly, so that it is possible to make a series of experiments on the drawing board. It is the author's conviction that the presented algorithm is useful for this purpose, even without further optimisation of the computer code.

6. Discussion. A direct or indirect use of the discretisation coordinates, in this case the end diameters of the conical segments, as design parameters makes the most flexible use of the discretisation. However, it was found impractical to optimise directly with respect to the discretisation coordinates.

As expected, the gradient based minimisation algorithm works best for intonation tasks, that is changes of the impedance spectrum that lead to moderate alterations of the geometry. However, in combination with parametrised models, it is possible to design musical horns from scratch.

The question about uniqueness and existence of solutions³ for which $J = 0$ is

³One-dimensional elliptic boundary value problems fall in the category of Sturm-Liouville equations. For a background on the existence and uniqueness of the solutions to inverse Sturm-Liouville problems, see for instance Borg [8]. An application of this theory with relevance to

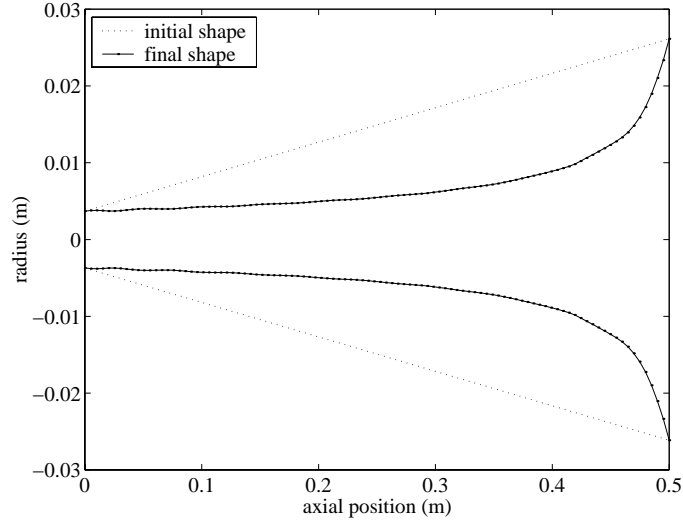


FIG. 20. *Horn geometry reconstructed using the two-pass location-level method.*

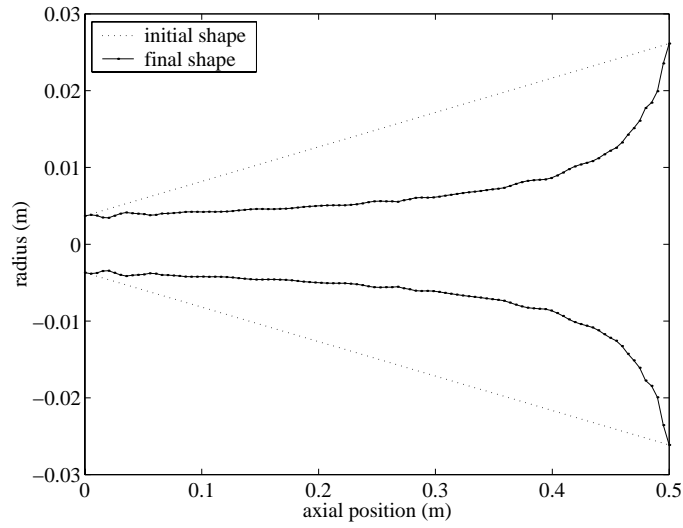


FIG. 21. *Horn geometry reconstructed using a two step gradual continuation method..*

important, but difficult to answer. For an intonation optimisation, the number of residuals, that is the number of terms in (1), is small compared to the number

musical acoustics is a paper by Gladwell and Morassi [14], which treats the inverse problem of determining the shape of a horn from its spectral properties.

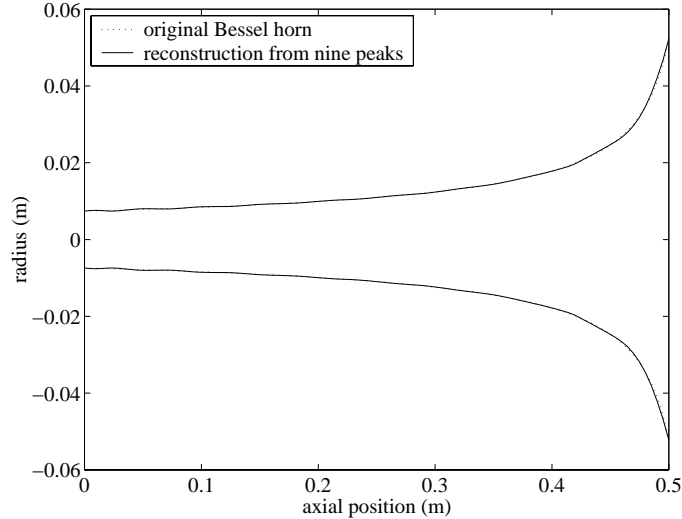


FIG. 22. Comparison between original shape, and the shape obtained by the two-pass location-level optimisation.

of design variables. It is therefore likely that the search space in many cases is large enough to include shapes for which $J = 0$. If this is the case it is also likely that there is no unique solution. No attempt is made here to study this question theoretically, but the numerical examples seem to indicate what is stated above.

If the number of design variables is smaller than the number of residual components, it is usually impossible to make J vanish. Furthermore, the object function (1) is generally not convex, whence only local solutions can be found by the minimisation algorithm used. This was demonstrated by the experiments.

It is remarkable that the reconstruction made from only impedance peak frequencies and levels works as well as it does, considering the small amount of information that is used. The similarity of the curves shown in Figs. 22 and 23 is striking.

The most notable limitations of the mathematical model used in this paper is the assumption that wave propagation can be described by the one-dimensional Webster equation, and the approximation of the radiation impedance at the mouth of the horn. For a rapidly flaring horn, higher order radially dependent modes have a significant influence on the impedance function. At low frequencies, most of the energy is reflected early in the horn, and higher order modes can be expected to be of subordinate importance. As the frequency rises, the waves reach further out in the flared bell, and modal conversion becomes increasingly significant. For a typical brass instrument, the impedance spectrum is affected considerably for the highest part of the playable frequency band. In order to include the effects of higher order modes, a number of different methods have

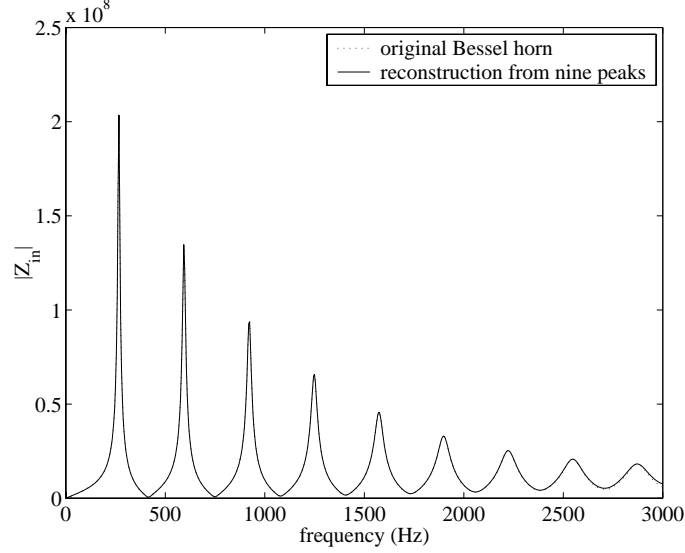


FIG. 23. Comparison between impedance spectra of original and reconstructed shapes as of Fig. 22.

been used. In [22] and [1], a multi-modal transmission line model is presented. In [12] and [3], the finite-element method is used for a more direct treatment of the wave equation in acoustic horns. These methods also include more general and accurate models for the radiation impedance. Future development of the algorithm presented in this paper might involve a hybrid between the transmission line model, and the finite-element method. A possibility is to work out an initial design using the former model, and then to perform a refined optimisation of the bell, using the latter model.

Acknowledgements. I am indebted to L. Abrahamsson and M. Berggren for their valuable input during the course of this work.

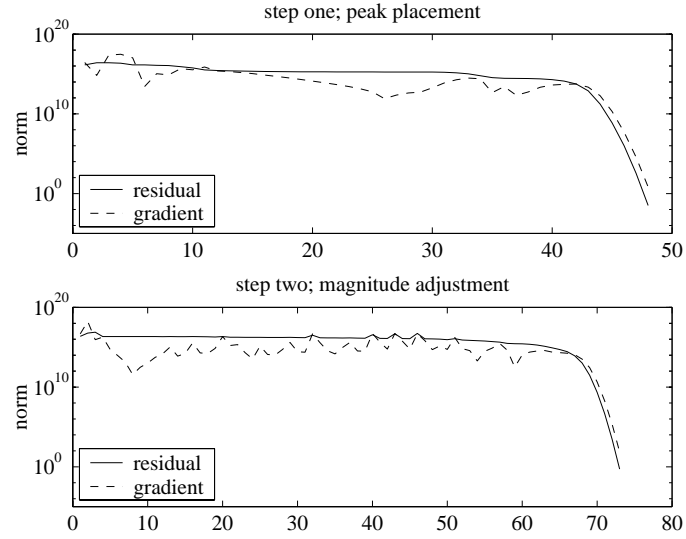


FIG. 24. Residual and gradient norms as a function of iteration count for the two respective steps of the location-level method.

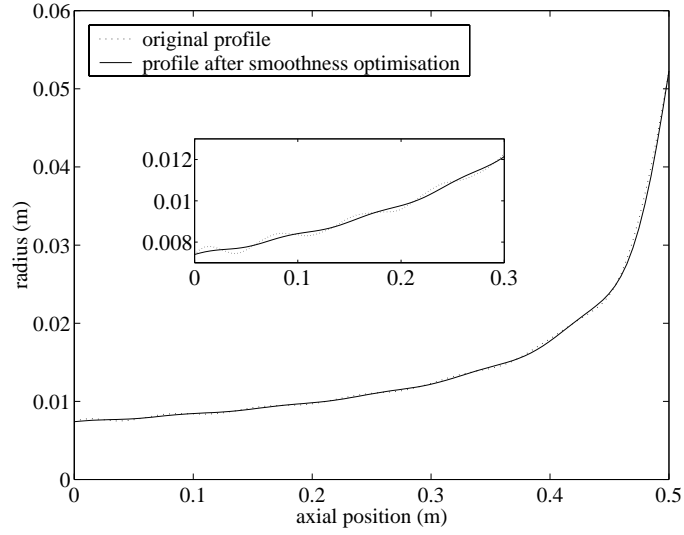


FIG. 25. Horn shape optimised w.r.t design smoothness and intonation imposed as an equality constraint. The inset shows a magnification of the “lead pipe”.

7. Appendix.

7.1. Transmission line elements of a cone. For a diverging lossy conical segment, the elements of the transmission matrix are

$$\begin{aligned}
 H_{11} &= \frac{L}{x_0} \left(\cosh(\Gamma\gamma) - \frac{1}{\Gamma L} \sinh(\Gamma\gamma) \right), \\
 H_{12} &= \frac{x_0}{L} Z_c \sinh(\Gamma\gamma), \\
 H_{21} &= \frac{1}{Z_c} \left\{ \left[\frac{L}{x_0} - \left(\frac{1}{\Gamma x_0} \right)^2 \right] \sinh(\Gamma\gamma) + \right. \\
 &\quad \left. + \frac{\gamma}{\Gamma x_0^2} \cosh(\Gamma\gamma) \right\}, \\
 H_{22} &= \frac{x_0}{L} \left(\cosh(\Gamma\gamma) + \frac{1}{\Gamma x_0} \sinh(\Gamma\gamma) \right). \tag{31}
 \end{aligned}$$

For a cylindrical tube of radius a , the complex wave number Γ and the complex characteristic impedance Z_c are given by

$$\begin{aligned}
 \Gamma &= k \left(\frac{1.045}{r_v} + \frac{1.080}{r_v^2} + \frac{0.750}{r_v^3} + \right. \\
 &\quad \left. i \left(1 + \frac{1.045}{r_v} \right) \right) \tag{32}
 \end{aligned}$$

and

$$\begin{aligned}
 Z_c &= Z_0 \left(\left(1 + \frac{0.369}{r_v} \right) + \right. \\
 &\quad \left. - i \left(\frac{0.369}{r_v} + \frac{1.149}{r_v^2} + \frac{0.303}{r_v^3} \right) \right), \tag{33}
 \end{aligned}$$

where

$$r_v = a \sqrt{\frac{\varrho \omega}{\eta}}. \tag{34}$$

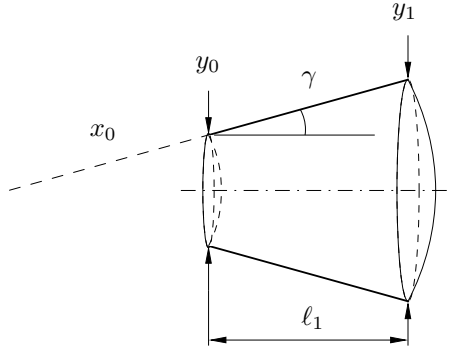
ϱ and η denote the density and the shear viscosity of air. $k = \omega/c$ is the free wave number. The quantity r_v is the ratio of the radius of the tube to the thickness of the viscous boundary layer. Table 7.1 lists the thermodynamic constants for the transmission line model.

In (32) and (33), r_v is evaluated for some “average” value of S . Throughout this work, r_v was evaluated at the centre of the truncated cone.

Entity	Value
c	$3.4723 \cdot 10^2 (1 + 0.00166\Delta T) \text{ ms}^{-1}$
η	$1.846 \cdot 10^{-5} (1 + 0.0025\Delta T) \text{ kgs}^{-1}\text{m}^{-1}$
ϱ	$1.1769 \cdot (1 - 0.00335\Delta T) \text{ kgm}^{-3}$

TABLE 4

Thermodynamic constants. ΔT is the temperature deviation from the reference temperature of 300K (26.85°C). Values are accurate at standard atmospheric pressure for $290\text{K} \leq T \leq 310\text{K}$.

FIG. 26. Dimensions used in the calculation of \mathbf{H} .

The following expressions, with dimensions defined by Fig. 26, were used in the calculation of 31:

$$\begin{aligned}
 \ell_2 &= (y_1 - y_0)/2 \\
 \gamma &= \sqrt{\ell_1^2 + \ell_2^2} \\
 x_0 &= \frac{y_0 \gamma}{2\ell_2} \\
 L &= x_0 + \gamma \\
 c_\theta &= \ell_1/\gamma \\
 S &= \frac{\pi y_0^2}{2(1 + c_\theta)} \\
 S_m &= \pi(y_0 + y_1)^2/16 \\
 r_v &= \frac{y_0 + y_1}{4} \sqrt{\frac{\rho\omega}{\eta}} \\
 Z_0 &= \rho c/S
 \end{aligned} \tag{35}$$

For a converging cone, the transmission matrix is given by

$$\mathbf{H} = \begin{bmatrix} H_{22} & H_{12} \\ H_{21} & H_{11} \end{bmatrix}$$

with elements as above.

7.2. Derivatives with respect to y_0 . In the present section, the $'$ -sign is short hand notation for d/dy_0 .

$$\begin{aligned}
l'_2 &= -1/2 \\
\gamma' &= \frac{\ell_2 \ell'_2}{\gamma} \\
x'_0 &= \frac{\gamma}{2\ell_2} + \frac{y_0 \gamma'}{2\ell_2} - \frac{y_0 \gamma \ell'_2}{2\ell_2^2} \\
L' &= x'_0 + \gamma' \\
c'_\theta &= -\frac{\ell_1 \gamma'}{\gamma^2} \\
S' &= \frac{\pi}{2} \frac{2y_0(1 + c_\theta) - y_0^2 c'_\theta}{(1 + c_\theta)^2} \\
S'_m &= \frac{\pi}{8} (y_0 + y_1) \\
r'_v &= \sqrt{\frac{\rho \omega}{16\eta}} \\
Z'_0 &= -\frac{\rho c}{S^2} S' \\
Z'_c &= Z'_0 \left(1 + \frac{0.369}{r_v} - i \left(\frac{0.369}{r_v} + \frac{1.149}{r_v^2} + \frac{0.303}{r_v^3} \right) \right) + \\
&\quad Z_0 \left(-\frac{0.369}{r_v^2} + i \left(\frac{0.369}{r_v^2} + 2 \frac{1.149}{r_v^3} + 3 \frac{0.303}{r_v^3} \right) \right) r'_v \\
G' &= -k \left(\frac{1.045}{r_v^2} + 2 \frac{1.080}{r_v^3} + 3 \frac{0.750}{r_v^4} + i \frac{1.045}{r_v^2} \right) r'_v
\end{aligned} \tag{36}$$

$$\begin{aligned}
H'_{11} &= \frac{-1}{x_0^2 \Gamma^2} (x_0 L' \Gamma^2 \cosh(\Gamma \gamma) + x'_0 L \Gamma^2 \cosh(\Gamma \gamma) - \\
&\quad x'_0 \Gamma \sinh(\Gamma \gamma) - L \sinh(\Gamma \gamma) \Gamma^2 x_0 \Gamma' \gamma - L \sinh(\Gamma \gamma) \Gamma^3 x_0 \gamma' - \\
&\quad x_0 \sinh(\Gamma \gamma) \Gamma' + x_0 \cosh(\Gamma \gamma) \Gamma \Gamma' \gamma + x_0 \cosh(\Gamma \gamma) \Gamma^2 \gamma')
\end{aligned}$$

$$H'_{12} = \frac{x'_0 L - x_0 L'}{L^2} Z_c \sinh(G \gamma) + \frac{x_0}{L} Z'_c \sinh(G \gamma) + \frac{x_0}{L} Z_c \cosh(G \gamma) (G' \gamma + G \gamma')$$

$$\begin{aligned}
H'_{21} = & -\frac{Z'_c}{Z_c} H_{21} + \frac{1}{Z_c} \left\{ \left[\frac{L'x_0 - Lx'_0}{x_0^2} + \frac{2}{\Gamma x_0} \frac{\Gamma'x_0 + \Gamma x'_0}{(\Gamma x_0)^2} \right] \sinh(\Gamma\gamma) + \right. \\
& + \frac{\gamma'\Gamma x_0^2 - \gamma\Gamma'x_0^2 - 2\gamma\Gamma x_0 x'_0}{\Gamma^2 x_0^4} \cosh(\Gamma\gamma) + \\
& + \left[\frac{L}{x_0} - \frac{1}{(\Gamma x_0)^2} \right] \cosh(\Gamma\gamma)(\Gamma'\gamma + \Gamma\gamma') + \\
& \left. + \frac{\gamma}{\Gamma x_0^2} \sinh(\Gamma\gamma)(\Gamma'\gamma + \Gamma\gamma') \right\}
\end{aligned}$$

$$\begin{aligned}
H_{22} = & \frac{x'_0 L - x_0 L'}{L^2} \left[\cosh(\Gamma\gamma) + \frac{1}{\Gamma x_0} \sinh(\Gamma\gamma) \right] + \\
& + \frac{x_0}{L} \left[\sinh(\Gamma\gamma)(\Gamma'\gamma + \Gamma\gamma') - \frac{\Gamma'x_0 + \Gamma x'_0}{(\Gamma x_0)^2} \sinh(\Gamma\gamma) + \right. \\
& \left. + \frac{1}{\Gamma x_0} \cosh(\Gamma\gamma)(\Gamma'\gamma + \Gamma\gamma') \right]
\end{aligned}$$

7.3. Some identities.

$$\begin{aligned}
\frac{d}{dy_0} \left(\frac{L}{x_0} \right) &= -\frac{y_1}{y_0^2} \\
\frac{d}{dy_0} \left(\frac{x_0}{L} \right) &= -\frac{1}{y_0} \\
\frac{d}{dy_1} \left(\frac{L}{x_0} \right) &= -\frac{1}{y_0} \\
\frac{d}{dy_1} \left(\frac{x_0}{L} \right) &= -\frac{y_0}{y_1^2}
\end{aligned}$$

7.4. Some limits.

$$\begin{aligned}
\lim_{y_1 \rightarrow y_0} \frac{d}{dy_0} \frac{1}{\Gamma L} &= -\frac{1}{\Gamma \ell_1 y_0} \\
\lim_{y_1 \rightarrow y_0} \frac{d}{dy_0} \frac{1}{\Gamma x_0} &= -\frac{1}{\Gamma \ell_1 y_0} \\
\lim_{y_1 \rightarrow y_0} \frac{d}{dy_0} \left(\frac{1}{\Gamma x_0} \right)^2 &= 0 \\
\lim_{y_1 \rightarrow y_0} \frac{d}{dy_0} \frac{\gamma}{\Gamma x_0^2} &= 0 \\
\lim_{y_1 \rightarrow y_0} \frac{d}{dy_1} \frac{1}{\Gamma L} &= \frac{1}{\Gamma \ell_1 y_0} \\
\lim_{y_1 \rightarrow y_0} \frac{d}{dy_1} \frac{1}{\Gamma x_0} &= \frac{1}{\Gamma \ell_1 y_0} \\
\lim_{y_1 \rightarrow y_0} \frac{d}{dy_1} \left(\frac{1}{\Gamma x_0} \right)^2 &= 0 \\
\lim_{y_1 \rightarrow y_0} \frac{d}{dy_1} \frac{\gamma}{\Gamma x_0^2} &= 0
\end{aligned}$$

7.5. Limits as $y_1 \rightarrow y_0$. Expressions (31)–(35) can be evaluated for $y_0 = y_1$ without modification, if the floating point representation contains `Inf`, but the corresponding derivatives must be evaluated analytically in the limit $y_1 \rightarrow y_0$. This yields

$$\begin{aligned}
H'_{11} &= -\frac{y_1}{y_0^2} \cosh(\Gamma\gamma) + \sinh(\Gamma\gamma)(\Gamma'\gamma + \Gamma\gamma') + \frac{1}{\Gamma \ell_1 y_0} \sinh(\Gamma\gamma) \\
H'_{12} &= \frac{1}{y_1} Z_c \sinh(\Gamma\gamma) + Z'_c \sinh(\Gamma\gamma) + Z_c \cosh(\Gamma\gamma)(\Gamma'\gamma + \Gamma\gamma') \\
H'_{21} &= -\frac{Z'_c}{Z_c^2} \sinh(\Gamma\gamma) + \frac{1}{Z_c} \left[-\frac{y_1}{y_0^2} \sinh(\Gamma\gamma) + \cosh(\Gamma\gamma)(\Gamma'\gamma + \Gamma\gamma') \right] \\
H'_{22} &= \frac{1}{y_1} \cosh(\Gamma\gamma) + \sinh(\Gamma\gamma)(\Gamma'\gamma + \Gamma\gamma') - \frac{1}{\Gamma \ell_1 y_0} \sinh(\Gamma\gamma)
\end{aligned}$$

7.6. Derivatives with respect to y_1 . The derivatives w.r.t y_1 are deduced in the same way. In the present section, the $'$ -sign is short hand notation for d/dy_1 . Only the terms that differ from the previous case are listed in the

following;

$$\begin{aligned}
 \ell'_2 &= 1/2 \\
 \gamma' &= \ell_2 \ell'_2 / \gamma \\
 x'_0 &= \frac{y_0(\gamma' \ell_2 - \gamma \ell'_2)}{2\ell^2} \\
 L' &= x'_0 + \gamma' \\
 c_\theta &= -\ell_1 \gamma' / \gamma^2 \\
 S' &= -\frac{\pi y_0^2}{2(1 + c_\theta)^2} c'_\theta
 \end{aligned}$$

REFERENCES

- [1] N. Amir, V. Pagneux, and J. Kergomard. A study of wave propagation in varying cross-section waveguides by modal decomposition. Part II. Results. *J. Acoust. Soc. Am.*, 101:2504–2517, 1997.
- [2] N. Amir, G. Rosenhouse, and U. Shimony. A discrete model for tubular acoustic systems with varying cross section - The direct and inverse problems. parts 1 and 2: Theory and experiment. *Acustica*, 81:450–474, 1995.
- [3] E. Bängtsson, D. Noreland, and M. Berggren. Shape optimization of an acoustic horn. *Computer Methods in Applied Mechanics and Engineering*, 192:1533–1571, 2003.
- [4] A. H. Benade. *Fundamentals of Musical Acoustics*. Dover Publications, New York, 1990.
- [5] A. H. Benade and E. V. Jansson. On plane and spherical waves in horns with nonuniform flare. i. theory of radiation, resonance frequencies, and mode conversion. *Acustica*, 31:79–98, 1974.
- [6] L. Beranek. *Acoustics*. McGraw-Hill, New York, 1954.
- [7] L. J. Bonder. Equivalency of lossless n-tubes. *Acustica*, 53:193–200, 1983.
- [8] G. Borg. *Eine Umkehrung der Sturm–Liouvilleschen Eigenwertaufgabe*. PhD thesis, Uppsala University, 1946.
- [9] A. M. Bruckstein, I. Koltracht, and T. Kailath. Inverse scattering with noisy data. *SIAM J. on Sci. Stat. Comp.*, 7:1331–1349, 1986.
- [10] A. M. Bruckstein, B. C. Levy, and T. Kailath. Differential methods in inverse scattering. *SIAM J. Appl. Math.*, 45:312–335, 1985.
- [11] R. Caussé, J. Kergomard, and X. Lurton. Input impedance of brass musical instruments—Comparison between experiment and numerical models. *J. Acoust. Soc. Am.*, 75:241–254, 1984.
- [12] R.-F. Fehlmann. *Computer Simulations and Application of Numerical Techniques for Acoustic Waves in Curved Swiss Horn*. PhD thesis, Norwegian Institute of Technology, Department of Telecommunications, Trondheim, 1994.
- [13] N. H. Fletcher and T. D. Rossing. *The physics of musical instruments*. Springer, New York, 1998.
- [14] G. M. L. Gladwell and A. Morassi. On isospectral rods, horns and strings. *Inverse Problems*, 11:533–554, 1995.
- [15] B. Gustafsson, H. O. Kreiss, and J. Oliger. *Time dependent problems and difference methods*. John Wiley & Sons, New York, 1995.
- [16] T. M. Kalotas and A. R. Lee. A new approach to one-dimensional scattering. *Am. J. Phys.*, 59:48–53, 1991.
- [17] W. Kausel. Optimization of brasswind instruments and its application in bore reconstruction. *Journal of New Music Research*, 30:69–82, 2001.
- [18] H. Levine and J. Schwinger. On the radiation of sound from an unflanged circular pipe. *Phys. Rev.*, 73:383–406, 1948.

- [19] D. Mapes-Riordan. Horn Modeling with Conical and Cylindrical Transmission-Line Elements. *J. Audio Eng. Soc.*, 41:471–483, 1993.
- [20] J. J. Moiré. The Levenberg-Marquardt algorithm: Implementation and theory. In G. A. Watson, editor, *Numerical Analysis*, pages 105–116. Springer Verlag, New York, 1977.
- [21] D. Noreland. A Numerical Method for Acoustic Waves in Horns. *Acta Acustica united with Acustica*, 88:576–586, 2002.
- [22] V. Pagneux, N. Amir, and J. Kergomard. A study of wave propagation in varying cross-section waveguides by modal decomposition. Part I. Theory and validation. *J. Acoust. Soc. Am.*, 100:2034–2048, 1996.
- [23] A. Papoulis. *The Fourier integral and its applications*. McGraw-Hill, 1962.
- [24] G. R. Plitnik and W. J. Strong. Numerical method for calculating input impedances of the oboe. *J. Acoust. Soc. Am.*, 65:816–825, 1979.
- [25] G. R. Putland. Every One-Parameter Acoustic Field Obeys Webster’s Horn Equation. *J. Audio Engineering Soc.*, 41:435–451, 1993.
- [26] S. W. Rienstra. The webster equation revisited. In *AIAA 2002-2520 of the 8th AIAA/CEAS Aeroacoustics Conference*, Breckenridge, Colorado, USA, June 2002.
- [27] G. Strang and G. J. Fix. *An Analysis of the Finite Element Method*. Prentice-Hall, Englewood Cliffs, NJ 07632, USA, 1973.
- [28] A. N. Tikhonov and V. Y. Arsenin. *Solutions to Ill-posed Problems*. Winston–Wiley, New York, 1977.